https://ntrs.nasa.gov/search.jsp?R=19730022104 2020-03-22T22:32:13+00:00Z

N73-30836

NATIONAL AERONAUTICS AND SPACE ADMINISTRATION

Technical Memorandum 33-599

Viking Orbiter 1975 Articulation Control Subsystem Design and Analysis

H. H. Horiuchi

L. J. Vallas

CASE FILE COPY

JET PROPULSION LABORATORY

CALIFORNIA INSTITUTE OF TECHNOLOGY

PASADENA, CALIFORNIA

July 15, 1973

NATIONAL AERONAUTICS AND SPACE ADMINISTRATION

Technical Memorandum 33-599

Viking Orbiter 1975 Articulation Control Subsystem Design and Analysis

H. H. Horiuchi
L. J. Vallas

JET PROPULSION LABORATORY
CALIFORNIA INSTITUTE OF TECHNOLOGY
PASADENA, CALIFORNIA

July 15, 1973

PREFACE

The work described in this report was performed by the Guidance and Control Division of the Jet Propulsion Laboratory, during the Subsystem development, January through October, 1971.

ACKNOWLEDGMENT

The authors wish to acknowledge Gerald S. Perkins who contributed the mechanical design data and pictorial illustrations for the scan, HGA, and SEC actuators.

CONTENTS

I. Introduction 1

II. Subsystem Design 3

A. Subsystem Requirements 3

B. Subsystem Design Concept 4

C. Subsystem Description 7

D. Mechanization 9

1. Input Unit 9

2. DAC and Error Detector 10

3. Dual Rate Motor Drive Pulse Generator 12

4. Digital Multiplexer and Motor Driver 14

5. Control Actuators 16

E. Scan Platform Settling Time 23

1. General 23

2. Settling Time Requirement 24

3. Mathematical Model 25

4. Simulation Results 28

F. Breadboard Test Results 29

G. Subsystem Errors 30

H. Production Proof Model. 31

TABLES

1. Functional requirements 32

2. System error tolerance requirements 32

3. Scan platform settling time requirements 33

4. ARTC telemetry outputs 33

5. CCS CC to ARTC 34

6. CCS DC for ARTC functions 36

TABLES (contd)

7. ARTC output selection logic 37
8. High/low slew mode selection logic 38
9. Timing values for signals in Fig. 19 38
10. Total errors contributed by ARTC electronics 39
11. Average dc power consumption for various operational modes 40
12. System scale factors and telemetry resolution 40
13. Motor winding grounding sequence 40
14. Stepper motor characteristics for scan actuator 41
15. Stepper motor characteristics for HGA and SEC actuators 41
16. Platform parameters 42
17. Summary of simulation runs 42
18. System test data at +25°C 43
19. Scan pointing errors (cone axis) 44
20. HGA and SEC control errors 45

FIGURES

1. Orbiter coordinate system 46
2. Scan platform system coordinate convention 47
3. HGA system coordinate convention 47
4. Simplified ARTC block diagram 48
5. Articulation control subsystem showing redundant control function 48
6. Equivalent system representation 48
7. Various redundancy schemes 49
8. Comparison of redundancy configurations 49

FIGURES (contd)

9. ARTC subsystem electronics block diagram 50
10. Input unit 51
11. Schematic diagram of ARTC input receiver 52
12. Signal timing diagram 52
13. Shift register clock position in the data field 53
14. CCS data format 53
15. Output selection logic and analog multiplexer 54
16. DAC and error detector 55
17. Motor drive pulse generator 56
18. Motor drive pulse sequencing 57
19. Delayed clock pulses and scan slew following latch set signal 57
20. ARTC/ACE interface circuit for scan slew signal 58
21. Scan slew signal with a turn-off delay 58
22. Digital multiplexer 59
23. Typical motor driver circuits and channel OR-ing scheme 60
24. Driver power distribution configuration 60
25. Alternate driver power distribution configuration 61
26. Schematic diagram of scan and HGA actuator 61
27. Schematic diagram of SEC actuator 62
28. Stepper motor schematic diagram 62
29. Size 15 stepper motor characteristics 63
30. Size 11 stepper motor characteristics 63
31. VO75 scan actuator 64
32. Clutch assembly scan actuator 65

FIGURES (contd)

33. VO75 antenna actuator 66

34. VO75 solar energy controller actuator 67

35. Simplified platform model 68

36. Near-in-phase transient response, 0.25-deg slew 68

37. Block diagram of simplified dynamics model 68

38. Platform settling characteristics 69

39. ARTC breadboard showing two control electronics channels and four actuators 72

40. Position error vs commanded position 73

41. ARTC electronics production proof model showing the module side 74

ABSTRACT

The Articulation Control Subsystem, developed for the Viking Orbiter 1975 spacecraft, is a digital, multiplexed, closed-loop servo system used to control the pointing and positioning of the science scan platform and the high-gain communication antenna, and to position the solar-energy controller louver blades for the thermal control of the propellant tanks. The development, design, and analysis of the Subsystem is preliminary.

The Subsystem consists of a block-redundant control electronics multiplexed among eight control actuators. Each electronics block is capable of operating either individually or simultaneously with the second block. This provides the Subsystem the capability of simultaneous two-actuator control or a single-actuator control with the second block in a stand-by redundant mode.

The result of the preliminary design and analysis indicates that the Subsystem will perform satisfactorily in the Viking Orbiter 1975 mission. Some of the parameter values used, particularly those in the Subsystem dynamics and the error estimates, are preliminary and the results will be updated as more accurate parameter values become available.

Overall Viking Project management is the responsibility of the NASA/ Langley Research Center; the Jet Propulsion Laboratory is developing the Orbiter System.

I. INTRODUCTION

The primary objective of the Viking program is to send two vehicles to the planet Mars to perform scientific experiments to advance the knowledge of the planet. This will include direct measurements in the atmosphere and on the surface and by observations of the planet during approach and from orbit. Two spacecraft, each consisting of an orbiter and a lander are planned for launch during 1975. Overall Viking Project management is the responsibility of the NASA/Langley Research Center; the Jet Propulsion Laboratory is developing the Orbiter System.

The Orbiter will transport and insert the Lander into Mars orbit and, prior to deorbit of the Lander, will map the surface with special emphasis on mapping the proposed landing site. After the Lander has landed, the Orbiter will relay telemetry data from the Lander to Earth. Scientific instruments on the Orbiter will be used to measure atmospheric and surface parameters at various times and locations to determine the dynamic characteristics of the planet.

The accomplishment of these scientific experiments will require accurate control of both the high-gain antenna (HGA) and the scan platform on which the scientific instruments are mounted. These bodies are controlled by the Articulation Control Subsystem (ARTC). The ARTC also controls the louver blade positions of four solar energy controllers (SEC); the blade positions provide the thermal control for the propulsion propellant tanks.

Figure 1 is a sketch of the Viking Spacecraft and shows the location of the scan platform and high-gain antenna. Figure 2 illustrates a coordinate system convention used for specifying scan platform angles, while Fig. 3 shows the antenna coordinate system.

As illustrated in Fig. 2, the scan platform is a two-degree-of-freedom structure. The platform clock axis allows rotation about an axis parallel to the spacecraft Z axis. The platform clock angle is the angle between the projection in the spacecraft X-Y plane of the platform line-of-sight (LOS) and that of the Canopus tracker LOS. The scan platform cone axis allows rotation of the platform about a line in the X-Y plane; the cone angle is the angle between the platform LOS and the spacecraft -Z axis.

The HGA is also a two-degree-of-freedom structure. The boresight direction of the antenna is defined relative to the spacecraft coordinate system in terms of azimuth and elevation angles. The azimuth axis is parallel to lines pointing at 270 deg in clock and 90 deg in cone; it is parallel to the plane of bay 3 as illustrated in Fig. 3. The elevation axis is normal to the azimuth axis.

In addition to these two articulating bodies, the spacecraft has four single-degree-of-freedom solar energy controllers, three of which are shown in Fig. 1. These bodies, consisting of eight control axes, are controlled through the Articulation Control Subsystem. A simplified ARTC block diagram is shown in Fig. 4.

The consolidation of similar subsystems not only reduces the hardware procurement cost, but also allows a major portion of the circuitry to be multiplexed or time shared among the various functions of the subsystems and results in a substantial hardware savings. Extensive use of microcircuits, monolithic integrated circuit amplifiers and digital elements, hybrid circuit analog switches, and a deposited film resistor network has yielded a low component count and accuracy difficult to attain with discrete components. The system requires no initial adjustment or component selection, operates using open-loop power supplies, and exhibits positioning accuracy consistent with 10-bit resolution.

Reliability is further enhanced by the system configuration that permits two modes of operation, either simultaneous two-axes control or single-axis control with the second channel in a stand-by redundant mode. This design is based on the condition that a single failure will not affect more than one output and if the failure is within the control electronics, single-axis control of all outputs is still possible. Each component that is common to more than a single output is provided with a redundant counterpart. The

actuators and the motor drivers that are provided with each output are not redundant; a failure here will cause the loss of only a single output. Redundancy to provide modes of operation after multiple failures is not included in the design.

II. SUBSYSTEM DESIGN

A. Subsystem Requirements

The functions of the Articulation Control Subsystem are constrained by the following requirements:

(1) The Subsystem must be capable of positioning eight output actuators by means of the Computer Command Subsystem (CCS) command.

(2) A single component failure within the Subsystem control electronics must not disable the slewing capability (except simultaneous two-axes slew capability) of any output actuator.

(3) The operating range and nominal commandable step size must be as shown in Table 1.

(4) The Subsystem must be capable of pointing the scan platform, the high-gain antenna, and the solar energy controllers as specified in Table 2.

(5) The Subsystem must be capable of slewing the scan platform in clock and cone axes sequentially or simultaneously.

(6) The scan platform slew rate must be selectable by the CCS command. The high slew rate is a minimum of 1 deg/s and the low slew rate is 0.25 deg/s.

(7) The scan platform settling time after the scan actuator has ceased its motion must be according to the requirements specified in Table 3.

Requirements 1 and 2 are the general system design requirements for the Subsystem. Requirements 3 and 4 specify the command input resolution, controllability, and control knowledge of the outputs. Requirements 5

through 7 specify the scan platform slew capability and constraints on its settling time.

The requirement of dual slew rate is based on the operational constraint of the scan platform. In certain slew modes, the platform is required to slew at a minimum rate of 1 deg/s. At this slew rate, it was discovered there is an interaction between the platform dynamics and that of the spacecraft structure resulting in an excessive use of attitude control gas. The requirement of a 0.25-deg/s slew rate was added to alleviate this problem so that the platform can be slewed at this lower rate at which the dynamic interaction of the bodies is less significant. Therefore, unless the platform is required to slew at a high rate, a low slew rate is used for the scan-slew operation. The slew rate of all other outputs is not a requirement, but a result of the scan-slew requirement and is summarized in Table 1.

The settling time of the scan platform is also a requirement based on the operational constraint of the scan platform. Table 3 shows the allowable maximum settling time after each platform slew as a function of slew angles. However, as it is discussed in detail later, the critical settling time for the Subsystem was found to be 4 s independent of slew angles. This is because the system slews at a constant rate independent of slew angles.

B. Subsystem Design Concept

Figure 4 is a simplified Subsystem functional block diagram and shows two independent channels of control electronics shared among eight outputs. The feedback signal from redundant potentiometers in the actuator is multiplexed into separate high-impedance, unity-gain, buffer amplifiers within each channel, while the digital outputs from each control channel are routed to the appropriate output driver through the digital multiplexer. Each control channel requires separate lines for the Computer Command Subsystem interface.

The design concept differs from the similar previous Mariner Control Subsystem in that multiplexing and redundancy are introduced. The initial design task was to develop a two-degree-of-freedom control subsystem for the scan platform. As the design evolved, it became apparent that with a small addition of circuitry, multiplexing of the control circuitry in a fashion that would provide functional redundancy could be accomplished. The Subsystem is mechanized with two independent control channels that are

multiplexed among the output actuators. The control channels provide the actuators with digital drive signals and receive analog feedback signals from them. The critical aspect of the design was in performing the multiplexing such that electronic failures do not interact between the control channels and that a single actuator failure does not affect other output functions.

The basic Subsystem structure shown in Fig. 5 illustrates the non-standby dual redundancy concept. In the diagram, channels A and B are two sets of identical control electronics and are functionally and electrically isolated from each other. The junction of the two control channels is mechanized such that operation of the Subsystem is possible regardless of any type of component failure in the control electronics. This was done by forcing the failure mode to be a high-impedance open circuit and never a direct short to either ground or a supply voltage. A detailed description of the circuitry is presented later.

The electrical isolation of the feedback signal between the two control channels is accomplished by using separate, mechanically coupled potentiometers. A separate feedback potentiometer is therefore provided for each control channel. This not only accomplishes the necessary isolation, but more importantly, provides a redundant feedback potentiometer.

A single actuator and a set of motor winding drivers are assigned to each output control function. Therefore, any component failure in this section will cause the failure of that output. Redundancy was not included in this section since even a minimum level of redundancy increases circuitry complexity and raises the weight and volume of the actuator substantially. Because of these hardware penalties, this was not pushed further.

The advantages of dual redundancy are fully utilized by assuring the isolation between the two control channels. This is further illustrated in the sample calculation that follows.

Referring to Fig. 5, since either channel A or B can perform independently of the other and also both channels can perform simultaneously, functionally the redundant system can be represented as shown in Fig. 6. Then the probability of events, P, for the Subsystem can be given by:

$$P = R_A R_B + R_A Q_B + R_B Q_A + Q_A Q_B$$

where:

R_A, R_B = the probability of success of channels A and B, respectively

Q_A, Q_B = the probability of failure of channels A and B, respectively

Here it is assumed that each electronics channel can perform satisfactorily or fail completely, thus leaving no possibility for an intermediate state.

The first term represents the probability that both channels survive; the second and third terms represent the probability that either channel can fail; the last term represents the probability that both channels fail. Therefore, the Subsystem failure probability Q_S of the redundant system is given by:

$$Q_S = Q_A Q_B$$

For the purpose of illustration, assume, $Q_A = Q_B = 0.01$. The Subsystem failure probability becomes $Q_S = 0.0001$. If the Subsystem is not assured of electrical isolation, a failure in one control channel can disable the function of the second channel: Q_S becomes $Q_X = 2(RQ) + Q^2 \simeq 0.02$. Thus, the advantage of providing the channel isolation is evident.

Figure 7 shows various redundant system configurations and their reliability expressions. λ is the failure rate of each subsystem block and is assumed constant. Figure 7a is a nonredundant system and is shown in comparison with the redundant systems. Figure 7b represents a nonstandby dual redundant system, whereas Fig. 7c represents a standby redundant system. The standby redundant system operates one subsystem block at a time by means of a block switching. The reliability expression assumes a perfect switching and does not account for the reliability of the switching function. Figure 7d represents a triple redundancy system in which the system functions until two of the three subsystem blocks fail. The Articulation Control Subsystem employs the redundancy scheme shown in Fig. 7b. The reliability expressions shown in Fig. 7 were plotted in Fig. 8 as a function of λt, where λ is assumed constant. The curves c and d show an advantage in reliability

over the curve b, but the added complexity in mechanization will become a disadvantage.

Another significant departure in the Subsystem design concept from previous articulation control subsystems, such as the Scan Platform Control Subsystem on the Mariner Mars 1971 spacecraft, is the use of stepper-motor actuator. The previous design employed a linear servo system using two-phase servo motors. The system required the reference windings of the motors be powered during slew and standby. The stepper motor, by its design, does not require the reference winding, and thus eliminated a significant portion of the servo power in the standby mode.

C. Subsystem Description

Figure 9 shows a function block diagram of the Articulation Control Subsystem. Since the control electronics channels A and B are identical, only channel A electronics is shown for description. For simplicity, eight motor drivers and eight actuators are combined into each functional block.

As shown, the Articulation Control Subsystem consists of the following functional blocks:

(1) Input unit.

(2) Digital-to-analog converter (DAC).

(3) Output address logic.

(4) Digital multiplexer.

(5) Analog multiplexer.

(6) Dual rate clock.

(7) Stepper-motor drivers.

(8) Stepper-motor actuators.

(9) Power supply.

This design uses a corrective mechanization in which the control error is corrected at discrete intervals and at a constant rate independent of error magnitude. Corrective action is initiated by the CCS command sequence. The command sequence starts with the transmission of a digital word that contains the output address and position information. Upon start of the command sequence, the input unit transmits the output address information to the

output address logic where the addressed output is identified. The input unit, simultaneously, transmits the output position information to the DAC where the position information in digital format is converted into an equivalent analog voltage. Upon receipt of the CCS strobe signal, a digital pulse signals the completion of the command sequence, and, if the parity of the data word has been verified, a latch circuit labeled SYSTEM-SET/RESET is set. This set signal allows the digital and analog multiplexers to activate their appropriate switches to close the control loop through the addressed actuator. The set signal also allows the dual rate clock to go into a time limited standby mode. The high or low slew rate is selected by a separate CCS command prior to a normal position control command.

Closing of the feedback loop through the analog multiplexer allows the error detector to compare the magnitudes of the command voltage at DAC output and the feedback voltage. Upon comparison of the voltages, the error detector determines the polarity of the error and issues a signal to the dual rate clock indicating the proper drive direction of the actuator. The clock, after the time limited standby period, issues a train of pulses properly sequenced to drive the actuator in the prescribed direction. When the clock pulses are transmitted to the actuator through the motor driver, the feedback signal is corrected at the rate of one step per clock pulse until the error crosses a null. When this occurs, the error detector changes state and resets the latch circuit. The Subsystem is at rest until the next sequence of CCS commands. The Subsystem employs the 2.4-kHz, 50-Vrms spacecraft power source. The Subsystem operation is synchronized to the various frequencies derived from the 2.4-kHz power source. Each actuator is provided with the telemetry potentiometer(s) to provide the actuator shaft angle information to the Flight Data Subsystem (FDS).

Table 4 lists the names of telemetry (TM) signals sent from ARTC to FDS. Tables 5 and 6 list the CCS Coded Command (CC) and Discrete Commands (DC), respectively; the CCs are sent directly to ARTC from CCS to control the ARTC articulation functions. The DCs are sent from CCS to other subsystems, such as the Power (PWR) and Pyrotechnic (PYRO) Subsystems, to effect the auxiliary functions related to the ARTC operations.

D. Mechanization

The detailed description of the electronics circuits is presented in accordance with the general functional breakdowns shown in Fig. 9. Since the two channels of the control electronics are identical, and each channel of the eight motor driver circuits are identical, one channel each of the control electronics and a driver circuit will be described.

1. Input Unit. The circuit contained in the input unit is shown in Fig. 10. The input unit receives the CCS CC sequence through the input receivers and stores the data word in the 14-bit shift register. The shift register provides a temporary storage of the command word until the next command sequence is received or the power is disabled.

The receiver, shown in Fig. 11, is used as an interface buffer to minimize the noise sensitivity of the subsystem's input circuitry. As shown in Fig. 11, the CCS CC signal is transmitted by the commutation of an isolated transistor switch. The interface signal level was selected to be 10 V to maximize the signal-to-noise ratio. The receiver input is a level detector that switches at +5 V with ±0.5-V hysteresis. The receiver output voltage level is limited to +5 V so that it is compatible with the transistor-transistor logic (TTL) circuits operating from +5 Vdc.

Figure 12, a timing diagram, shows the sequence of CCS CC signals: Enable, Data, and Strobe. The Enable, a discrete signal that brackets the data field, is 15-bit-time long and enables a two-flip-flop counter, I_1 and I_2, and generates a 208-μs, 1.2-kHz clock pulse. Since this clock pulse is derived from the spacecraft 2.4-kHz power source, it is in synchronism with the CCS CC signal and used to clock the data in. A unique feature of the circuit is that regardless of the edge of the 2.4-kHz reference to which the CCS data is synchronized, the 1.2-kHz clock pulse is positioned in the third quadrant of each data bit as shown in Fig. 13. This allows the switching transient a maximum of 416 μs.

The Data line, which contains 10 bits of position information, three bits of output address information and one parity bit, is received at 1.2-kHz rate in a nonreturn-to-zero (NRZ) format.

Figure 14 shows the CCS CC date word format and Table 7 shows the coding of the output address bits. The corresponding address decoding circuit, connected to the analog multiplexer switch, is shown in Fig. 15.

As shown in Fig. 12, the Strobe occurs at the end of the data field, in bit-time 15, and is used to generate a strobe clock that checks an odd parity of the data word. When the parity is verified, a Latch-Set signal is issued to the latch circuit and resets the error detector flip-flops shown in Fig. 16. The error detector flip-flops, when reset, enable the latch circuit, thus setting the System-Enable/Disable output to System-Enable. This signal indicates that the CCS CC sequence has been completed and the Subsystem is ready for slew.

2. DAC and Error Detector. Figure 16 is a diagram of the 10-bit DAC and error detector. The DAC uses a 1-in.-square deposited film resistor network.

The network contains a 12-bit, 20-kΩ, R-2R ladder, three application resistors, and exhibits a maximum output voltage ratio error of ±122 ppm (±0.012%) over the temperature range of -55°C to +125°C. The use of this commercially available network virtually eliminates the ladder and summing resistors as sources of error. The output of the ladder is buffered by an inverting amplifier with a gain of two and summed with the feedback voltage. Mechanized this way, the DAC and feedback voltages track, volt-to-volt, as a function of reference voltage variation. This greatly simplifies the design of the reference supplies and allows open loop ±6.2-V zener diode regulators to be used.

The reference voltage levels were determined by a trade-off study between minimizing the effects of initial offset voltages and their associated temperature drift against the added circuit complexity needed to accomodate higher voltages. The levels of ±6.2 V were chosen, since higher levels would require increased complexity in the DAC inverting amplifier without appreciably improving overall Subsystem accuracy.

The DAC switches that alternately switch +6.2-V reference or -6.2-V reference to the ladder network are required to have low saturation resistance and offset voltages. Figure 16 shows the Siliconix DG 186, a hybrid circuit containing a single bipolar integrated circuit driver and two discrete n-channel junction field effect transistors (FETs). The DG 186 is a DG 187

modified by using low resistance FETs as compared to the normal 30-Ω devices. The drivers are designed to operate in a break-before-make mode, thereby preventing large current spikes during the switching transient. These drivers can interface with the TTL circuit and hence are actuated directly from the binary shift register. The channel resistance is 10 Ω and hence, in the one state, the FET is a simple ohmic resistance; it has no offset voltage.

The low channel resistance is obtained by using large geometry FET devices and, as a consequence, they have a substantial leakage current of 0.064 μA maximum at 85°C. While the leakage current has an adverse effect in many applications, the DAC switch, because of its push-pull configuration, is unaffected.

The Subsystem functional diagram shows the analog feedback signals multiplexed into a single noninverting unity gain amplifier. The amplifier, which functions as a high input impedance buffer, prevents loading of the feedback signal source and reduces the effect of the multiplexer impedance to negligible proportions. The Siliconix DG 133, which is similar to Siliconix DG 186, is used as the multiplexer. The low drain-to-gate-leakage current, 1 nA maximum at 25°C, makes this device ideal for use as an analog multiplexer. The significant sources of error are the amplifier offset voltage and the leakage current of the switches. To reduce the effect of the leakage, 5-kΩ feedback potentiometers are used. This lowers the signal source impedance to 1.25 kΩ maximum.

The error signal that results from the difference of the ladder output and feedback voltages is detected by a LM 108A integrated circuit amplifier and a dual J-K flip-flop connected to form a null detector. Even though the impedance level of the summing junction is high, 13.3 kΩ, the extremely small bias currents of the LM 108A makes additional buffering unnecessary. Consequently, errors due to temperature associated current drifts can be neglected. The error detector outputs are used to generate three logic signals; the count-down and count-up signals that control the reversible counter shown in Fig. 17, and the system inhibit signal. At the beginning of a slew after parity verification, the flip-flops are cleared by the Logic-Reset signal. At the end of the slew, depending on the polarity of the error signal, one of

them will change state when a null is detected. The signal resets a latch turning the system off until the next CCS command is received.

Analog errors at the summing junction are reflected to the output by a 3/2 factor. The primary source of error is initial input voltage and current offsets and their temperature associated drifts. The use of the LM 108A, a monolithic integrated circuit amplifier that is designed with super gain transistors as its input, provides the input bias and offset currents of levels less than 2 nA. By careful selection, the manufacturer guarantees an initial offset voltage of less than 0.5 mV and a temperature drift of less than ±3 μV/°C. The use of this device with its excellent input characteristics not only allows the drift errors to be neglected, but eliminates the need for component selection and initial adjustment.

3. Dual Rate Motor Drive Pulse Generator. Figure 17 shows the dual rate motor drive pulse generator that consists of a clock generator, a 2-bit reversible counter, and a pulse sequencer. The high-rate pulses are generated at 100 pulses/s and the low-rate at 25 pulses/s.

The clock generator is a 7-bit ripple counter connected to divide the system's 2.4 kHz by 24 to provide a 100-Hz pulse. The pulse width is 416 μs. The 2-bit reversible counter and the pulse sequencer, depending on the polarity of the error signal from the error detector output, issue the clockwise or counterclockwise pulse sequence to the motor drivers. The pulse timing diagram is shown in Fig. 18. The flip-flops I_1 and I_2 are clocked J-K elements. The clock pulses are normally inhibited and are enabled by the System-Enable signal when its control channel is addressed.

Selection of a 100-Hz or 25-Hz pulse rate is made by a CCS CC as shown in Table 8. The high-rate slew mode, corresponding to the 100-Hz pulse rate, is selected when SEC 4 output is addressed accompanied by a logical 1 in the least significant bit (LSB) of the position information. In this state, the Subsystem slew is inhibited and the flip-flop I_3 is clocked so that its output Q_3 becomes a logical one. This allows the summing gate G_1 to close the loop through G_2, which resets the flip-flop I_4 every 24 pulses. A 100-Hz pulse is generated at the output of the gate G_2.

Similarly, the low-slew-rate mode, corresponding to a 25-Hz pulse rate, is selected when SEC 14 output is addressed and accompanied by a

logical 1 in the least significant bit of the position information. The Subsystem slew is inhibited and Q_3 is set to a logical zero. This disables the gate G_1 and allows the ripple counter to close the loop through the flip-flops I_5 and I_6. In this mode, the gate G_2 resets the flip-flop I_4 every 96 pulses thus generating a 25-Hz pulse at the output of the gate G_2.

As shown in Table 8, when the SEC output is addressed for a normal position control, the LSB is set to a logical zero. Although this preassigned logical state introduces an offset in the commanded position, this has no impact on the SEC operation since only 6-bit resolution is required for the SEC position control.

The flip-flop I_7, after reset by the Latch-Set signal, holds the error detector flip-flops I_1 and I_2 in Fig. 16 in the cleared state. The clear state lasts for two clock periods following the latch set signal: 20 ms for a high-rate slew mode and 80 ms for a low-rate slew mode. This inhibit period is necessary to avoid a premature setting of the error detector flip-flops by the noise transients at the error detector input. This transient noise is due to the multiplexer switching in the feedback network following the System Enable signal and lasts about 1 ms. Figure 19 is a timing diagram showing the time delay introduced by the flip-flop I_7 prior to the generation of the clock pulse. Table 9 lists the timing values for Fig. 19.

The time delay provided by the flip-flop I_7 also satisfies a timing requirement for Scan Slew signal to the Attitude Control Electronics (ACE). The leading edge of the Scan Slew level signal generated by the output selection logic, shown in Fig. 15, must be transmitted to the ACE before the start of the scan actuator slew. This signal is used in the ACE to set the attitude control logic to a scan slew configuration. There is an 8-ms transport delay through the interface circuitry between ARTC and ACE. A 20-ms delay provided by I_7, therefore, ensures the interface timing requirement. The Scan Slew start signal is shown in Fig. 19 and the interfacing circuit is shown in Fig. 20. The design of the ACE signal receiver is identical to that used in the ARTC-CCS interface shown in Fig. 11.

The ACE control logic also requires the Scan Slew signal to remain on for two additional seconds after the completion of a scan slew. This is to ensure that a post-slew resetting of ACE control logic is accomplished after the scan platform settling transient has subsided. The platform settling time

has been estimated to be below 1 s for nominal system parameters. Figure 21 is a timing diagram showing the 2-s delay between the System Enable/Disable and Scan Slew signal at the termination of a scan slew. As shown in Fig. 20, a cascaded transistor stage provides a discharge time constant large enough to sustain the scan slew signal for two additional seconds.

Redundancy is not provided in the ARTC-ACE interfacing circuitry. Therefore, a failure in the common circuit where the Scan Slew signals from the redundant control channels are OR-ed can disable the transmission of the Scan Slew signal to ACE. This failure mode, however, was considered non-critical from the operational standpoint of Attitude Control Subsystem function.

Table 10 is the result of an error analysis. The $\pm 3\text{-}\sigma$ error is ± 5.34 mV or $\pm 0.043\%$ full scale as compared to the worst case of $\pm 0.074\%$. The dispersion factor, σ, was found by assuming that the individual component errors are uniformly distributed about their nominal value and bounded by their maximum specification limit. The variance of a sum of random variables is found by summing the individual variances and the density function by convolving the individual density functions. Since the convolution of a large number of independent density functions results in a normal distribution, the square root of the sum of the variances is the dispersion factor of the normal distributed error function.

4. Digital Multiplexer and Motor Driver. The digital multiplexer circuit is shown in Fig. 22. The multiplexer receives the motor drive pulses from the dual-rate pulse generator and channels them to the selected motor driver. The input to each motor driver forms a junction where the corresponding multiplexer output from two control channels are OR-ed. Therefore, a critical design consideration for the multiplexer driver interface is the implementation of the OR-ing function between the two control channels such that a failure in one multiplexer output will not preclude the operation of the remaining channel. This requires that the failure mode at the channel outputs be an open circuit. Several interface configurations were considered and trade-off studies were made. The primary trade-off factors were the power consumption and the circuit complexity. When the design was optimized for the minimum standby power employing low-power TTL

elements, the driver circuit required more stages of amplification to produce the required output drive capability. When the driver circuit design was optimized for the least number of parts count, an increased driving capability was required of the multiplexer interface. The selected interface configuration is illustrated in Fig. 23, showing one of the four motor winding drivers. Since there are four motor windings to be energized in a sequence for the motor to be driven in a direction, a motor driver consists of four motor winding drivers. This design was selected for its circuit simplicity resulting in the minimum parts count. This configuration also satisfies the required OR-ing between two control channels.

Figure 22 shows a set of outputs from the multiplexers of channels A and B. Each output from the multiplexer is buffered by SN5406, as shown in Fig. 23, before it is connected to the corresponding motor winding driver. The output stage of SN5406 is a transistor with an open collector configuration. This allows the diode OR-ing of the two corresponding multiplexer signals from channels A and B at the input to the motor winding driver. When the Subsystem is in a standby mode where no slewing takes place, the output transistors of SN5406 are saturated, thus keeping the OR-ing diodes back biased. Under this condition, the driver transistors Q_1 and Q_2 are turned off. When the Subsystem is in a slew mode, the four motor windings of the selected actuator are sequentially energized. Under this condition, the output transistors of SN5406 are sequentially turned off for 10 ms for high-rate slew and 40 ms for low-rate slew. When the SN5406 output transistor is off, driver transistor Q_1 is saturated by receiving a bias current through a 1-kΩ pullup resistor and the diode. Q_1 supplies the base current to Q_2, and Q_2 is saturated. Since the collector of Q_2 is connected to the +28 Vdc supply through a motor winding, that winding is energized.

Although the scan actuator requires a size 11 stepper motor and the HGA and SEC actuators require a size 8 stepper motor, an identical circuit design was used for all drivers to simplify the design effort and manufacturing processes. Therefore, the circuit was designed to be capable of driving the heaviest load. The driver was designed to drive a size 11 stepper motor, which draws a nominal peak current of 280 mA. Thus, the same driver can drive a size 8 motor, which draws a nominal peak current of 150 mA.

Cordwood construction technique is being planned to package the driver circuit. This approach offers a high-density package as well as a plug-in feature. The combination of uniform design and plug-in feature allows an efficient utilization of spare driver units.

Figure 24 shows the Subsystem power distribution configuration for the +28 Vdc supply used in powering the driver circuits and the stepper motors. The two +28 Vdc supplies are diode OR-ed, so that in case of a failure in one +28 Vdc supply, the other supply can continuously power the drivers and motors. Each +28 Vdc supply was designed to supply currents required for simultaneous slewing of two size 11 motors. Therefore, a failure in one +28 Vdc supply will not affect the Subsystem's capability to slew two scan platform axes simultaneously. Each driver is powered through a fuse in the +28 Vdc line. The fuse size was selected so that it opens the power line to the driver only when a catastrophic failure such as an electrical short occurs in the driver circuit, the cable, or the motor. The use of fuses in the power line is necessary to protect the common +28 Vdc power source from being shorted to ground, thus disabling the entire Subsystem functions. An alternate mechanization would be to eliminate the diode OR-ing and assign each of the +28 Vdc supply to certain drivers and their corresponding motors. This approach is illustrated in Fig. 25. Clearly this mechanization has a disadvantage of disabling a half of the output control axes in case one of the +28 Vdc supply is disabled. This mechanization, however, presents no critical common power distribution point as in the first mechanization, and thus requires no fuses. In the present design of the Articulation Control Subsystem, the first mechanization has been selected as it can offer a greater versatility in power distribution to the drivers. The critical common point, where the two +28 Vdc supplies are diode OR-ed and power distribution through the fuses occur, can be made physically compact thus minimizing the chance of shorting.

The average power consumptions for various operational modes are summarized in Table 11.

5. Control Actuators.

a. General description. The Articulation Control Subsystem requires eight control actuators to articulate the various loads on the

spacecraft. There are two scan actuators, two high-gain antenna actuators and four solar energy controller actuators.

The two scan actuators are designed to be identical and thus, interchangeable. One actuator is installed in the scan clock axis gimbal and the other in the cone axis gimbal. The two HGA actuators are designed to be identical and thus, interchangeable. One actuator is installed in the azimuth axis gimbal and the other in the elevation axis gimbal. The four SEC actuators are designed to be identical and thus, interchangeable. Each actuator is installed in one of the four solar energy controller assemblies that are located in the near vicinity of the propulsion fuel tanks.

Schematic diagrams of scan, HGA, and SEC actuators are presented in Figs. 26 and 27. All actuators employ a stepper motor and a conventional gear grain mechanism to obtain the required torque level and speed at the output shaft.

Each actuator is installed with a potentiometer or a set of potentiometers to supply the output shaft position information to the Flight Data Subsystem on the spacecraft. Since the output shaft is directly linked to the articulated load, the telemetry potentiometer reading indicates the position of the load in a given control axis. The Flight Data Subsystem provides a resolution of 7 bits, or 128 divisions, for a given measurement. Thus, the telemetry resolution of a potentiometer output is one part in 128. The SEC actuator that requires the output position resolution of 6 bits, or 64 divisions, is provided with one telemetry potentiometer. The full range of the potentiometer is made to correspond to the full range of the SEC output angle. Thus, one increment change in the SEC output position will indicate a change in a telemetry reading of two increments. The scan and antenna actuators that require an output position resolution of 10 bits, or 1,024 divisions, is installed with two potentiometers. One potentiometer, called the course telemetry potentiometer, is used in a similar way as the SEC telemetry potentiometer and has a resolution of one part in 128. The second potentiometer, called the fine telemetry potentiometer, is used as a vernier on the coarse potentiometer. The fine potentiometer wiper turn rate is stepped up relative to the coarse potentiometer through a gear train N_3 so that one complete revolution of the fine potentiometer corresponds to a small fraction of a full range on the coarse potentiometer. Since the fine potentiometer

also has a telemetry resolution of one part in 128, the resolution of the fine telemetry potentiometer relative to the full scale on the coarse potentiometer becomes $K \times 1/128$, where K is a fraction of a full scale on the coarse potentiometer, which corresponds to one revolution of the fine telemetry potentiometer. The telemetry resolution of each actuator is summarized in Table 12.

In each of the actuators is installed two feedback potentiometers mechanically coupled to the coarse telemetry potentiometer. The feedback potentiometer provides a shaft angular position in the form of an analog voltage, whose magnitude is proportional to the actuator output shaft angular position. Since the Subsystem consists of two separate channels of control electronics, each feedback potentiometer is connected to its assigned channel. When the Subsystem is in slew, the feedback voltage is continually compared with the command reference voltage from the output of the DAC in the control electronics. When the load angular position reaches the commanded position, the two voltages, the feedback and the DAC output, will produce a null into the error detector, and thus the control loop for this output is disabled. The feedback potentiometer has a minimum electrical angle of 350 deg. A full load angular range varies from 230 deg for the scan clock axis to 90 deg for the SEC control axis. To optimize resolution on the potentiometer, the feedback potentiometer wiper is stepped up through the gear train N_2 so that a full load angular range corresponds to an angle on the potentiometer that is close to 350 deg. The scale factors of the feedback and telemetry potentiometers are summarized in Table 12.

A permanent magnet 4-phase stepper motor has four control windings. When each of these windings is energized in certain sequences, the stepper motor rotates in either clockwise or counterclockwise direction in discrete step angles. Since the motor employed in this design has a step angle of 90 deg, one sequence of energizing four windings rotates the motor shaft by 360 deg or one complete revolution. A schematic diagram of a typical 4-phase stepper motor is shown in Fig. 28, and the sequence in which the motor windings are energized is summarized in Table 13. When a stepper motor is driven by a driver, each motor winding terminal (W1 through W4) is grounded by closing a corresponding transistor switch in the driver, thus energizing the motor winding. Therefore, the driver circuit has a set of

four such switches that open and close according to the sequence shown in Table 13.

Detailed descriptions of the scan, HGA, and SEC actuators are presented in the following subparagraphs. Each type of actuator has been designed to satisfy its own requirements. An attempt to make all actuators identical with a uniform design was considered impractical not only from a standpoint of cost, weight, and volume, but also of functional design as well.

b. Scan actuator. A schematic diagram of the scan actuator is shown in Fig. 26. The scan actuator is required to perform with the following functional constraints:

(1) The clock and cone actuators must be interchangeable.

(2) The actuator must be capable of functioning over a full range of 230 deg in the clock axis and 170 deg in the cone axis.

(3) The actuator must be capable of slewing the platform at a minimum rate of 1 deg/s.

(4) The actuator must be capable of maintaining its stationary position during the thrust phase of the spacecraft maneuver.

The first and second constraints can be met by designing an actuator with a full output range capability of 230 deg. The cone axis, which has a narrower output range, can be accommodated by using a portion of the full range.

However, the scan system is provided with a 10-bit commandable resolution and is required to increment the output position by a multiple of 0.25 deg. Since a 10-bit resolution provides 1023 increments in the DAC, the total available shaft angle range at 0.25-deg increments is 255.75 deg. It was decided to design the scan actuator with this operating range, which is wider than the presently required range of 230 deg because it provides the nominal command resolution of 0.25 deg and also can accommodate a change in the operating range without affecting the actuator design. The maximum operating range is thus determined by the CCS command word structure.

The third and fourth constraints require an investigation of the stepper-motor characteristics and the motor performance assessment under the platform load. The moment of inertia of the platform is estimated to be

between 13.6 and 20.3 kg-m^2. Under a zero g condition, a minimum of 0.57 N-m of drag torque is estimated in the platform bearings. To increase the Subsystem damping to minimize the scan platform settling time, an additional 1.1 to 1.7 N-m was added by preloading the platform bearings. Therefore, a maximum load for the scan actuator is represented by an inertia load of about 20.3 kg-m^2 and a bearing drag torque of about 2.3 N-m.

A study of the stepper-motor characteristics was made using a permanent magnet motor with a 90-deg step angle. Typical characteristics of the motor torque vs step rate and the corresponding inertia loading capability of the motor for sizes 11 and 15 are shown in Figs. 29 and 30, respectively. Parts (a) show a torque vs maximum response rate of the motor. Maximum response rate is defined here as the maximum input pulse rate at which a stepper motor can start, follow, and stop without missing a step. Parts (b) show the inertia loading capability of the motor as a function of step rate.

The scan actuator is required to slew at a minimum rate of 1 deg/s in a high-rate mode. If a permanent magnet motor with a 90-deg step angle is chosen, the ratio of the gear ratio N to the step rate K, as shown in the following relation, becomes 90.

$$(90 \text{ deg/step})\ (K \text{ steps/s})\ \frac{1}{N} = 1 \text{ deg/s}$$

If a step rate of 100 steps/s is chosen, the required gear ratio N is 9000, and the resulting actuator shaft angle increment is 0.01 deg. The size of the angle increment was considered adequate considering a required nominal output increment is 0.25 deg. A breadboard investigation showed that the stepper motors of size 11 and 15 categories produce a near-linear angular motion when stepped at 100 steps/s with a near-100% duty cycle. The stepping rate of 100 steps/s was assumed as a reference operating point of the motor in the following analysis. Referring to parts (a) of Figs. 29 and 30, in addition to a typical and a minimum curves, a curve representing a friction load of 3.5×10^{-4} N-m at the motor shaft is shown as a reference. This load represents a friction torque of 2.3 N-m at the actuator assuming an actuator torque transmission efficiency of 70%. Parts (b) show the allowable total inertia, the sum of the reflected and the motor inertias, as a function of the motor's maximum response rate. All three curves in each

part (b) correspond to the respective curves in the torque vs step rate shown in parts (a). For example, if a size 11 motor is operated at 100 steps/s, a friction load of 3.5×10^{-4} N-m reduces the total allowable inertia at the motor shaft by about 0.83 g-cm^2, or the total inertia allowed is about 5 g-cm^2 including the rotor inertia.

When the rotor inertia of 1 g-cm^2 is subtracted, the allowable reflected load inertia becomes 4 g-cm^2. This figure may be compared with the reflected load inertia of 2.5 g-cm^2, which represents an assumed scan load inertia of 20.3 kg-m^2 at the actuator shaft. Thus, a margin of the inertial load of capability is 1.5 g-cm^2.

A summary of the motor characteristics is presented in Table 14. The size 11 and size 15 motors apparently satisfy the overall requirements for the scan application. However, as shown in the Table 14, the size 15 motor can offer a far better design margin. On the other hand, the size 15 motor is 3 times heavier and consumes about 70% more power. A size 11 motor has been selected for the scan actuator.

A pictoral presentation of the scan actuator is shown in Fig. 31. Initially the worm gear was considered necessary to keep the platform stationary when the Subsystem power is off during the spacecraft maneuvers in flight. The magnetic detent torque of the motor, which amounts to about 10 to 20% of the motor stall torque, is sufficient to hold the platform in position during the above spacecraft activities. One gearing away from the output shaft, a slip clutch is installed. The slip torque of the clutch is set such that it is less than the reflected detent torque of the motor at the clutch, but greater than the minimum required torque to hold the platform in position during the thrust phase of the spacecraft maneuver. Without the slip clutch in the actuator, the stepper motor can be accidentally backdriven by turning the platform during ground test. If the turn rate of the platform is high enough, the motor turns at prohibitively high rpm and can be damaged. The slip clutch protects the motor and gears by slipping the clutch at preset torque levels. The slip clutch will not slip when the scan platform is inadvertently driven against the platform mechanical stops. Under this condition, the motor will be stalled. The slip torque level was selected to be between 23 N-m and 45 N-m referenced to the output shaft. This is

considered adequate since the detent torque reflected at the output shaft is estimated to be about 27 N-m. The slip clutch is illustrated in Fig. 32.

c. HGA actuator. Figure 33 is a pictorial presentation of the HGA actuator. The two HGA actuators control the positioning of the high gain antenna in the elevation and the azimuth axes. The required operational angular range differ between the two control axes. The operational angular range of the azimuth actuator is 181 deg and that of the elevation actuator is 200 deg. Thus, the actuator is designed for a full range of 200 deg. The azimuth range of 181 deg can be accommodated by using a portion of the available 200 deg on the actuator.

The HGA control system is provided with a 10-bit command resolution and required to increment the output position by a multiple of 0.2 deg. Since a 10-bit resolution provides 1023 increments in the DAC, the total available shaft angle range is 204 deg.

The antenna actuator is required to drive a considerably less load inertia than the scan actuators. An estimated load inertia at the antenna azimuth drive axis is a maximum of about 2.7 kg-m^2 and that of the elevation drive axis will be less. The friction torque in the hinges is estimated to be less than 0.57 N-m. There is no specific constraint on the slew rate of the antenna. After the initial deployment, the antenna position in either one or both axes will be updated daily by one increment or about 0.2 deg. Thus, there exists no settling time constraint on the antenna dynamics and consequently there is no requirement for preloading the antenna hinge axes bearings as in the scan platform to produce an effective damping. As in the case of the scan actuator, the antenna actuator is required to hold the load in position during the thrust phase of the spacecraft maneuver.

Considering the functional constraints described, especially inertia loading, a size 8 stepper motor was selected to be used. With a gear ratio of 9000, a permanent magnet size 8 motor with a 90-deg step angle will yield a 0.01-deg step angle at the actuator output shaft. This step size was considered reasonable when it is compared with the increment size of 0.2 deg. Since all control loops in the Subsystem are closed through a common control electronics, the stepper motor in the HGA actuator is stepped at the same rate as the scan stepper motor, at 100 pulses/s in a high-slew-rate mode and at 25 pulses/s at a low-slew-rate mode. At 100 steps/s, the

motor produces about 8.4×10^{-4} N-m drive torque. With an estimated torque transmission efficiency of 70%, the actuator produces about 5.3 N-m of torque at its output shaft. The inertial loading capability of the motor is about 1.3 g-cm^2. When reflected to the actuator output, it represents 10.4 kg-m^2 of load inertia capability with 0.57 N-m of friction load. In the antenna actuator, as in the scan actuator, a slip clutch is installed to protect the stepper motor from being damaged by backdriving through the antenna structure. The slip torque setting for the clutch was based on design considerations similar to those for the scan slip clutch. The slip torque value at the output shaft is set between 9 and 18 N-m.

d. SEC actuator. The SEC actuator is illustrated in Fig. 34. Each of the four actuators controls the positioning of the louver blades in the SEC assembly. The four SEC assemblies are used to control the surface temperature of the propellant tanks by controlling the amount of reflected solar energy on the tank surfaces.

The four actuators are of identical design and interchangeable. The operating range of the actuator is 90 deg for all actuators.

The SEC control system has a command input resolution of 6 bits, or 63-DAC increments. Since the operating range is 90 deg, the output shaft is updated in increments of 1.43 deg.

An estimated friction load for the SEC actuator is about 7×10^{-2} N-m and an estimated inertia load of less than 1000 g-cm^2. Referring to Table 15, it is seen that these figures represent a very negligible loading on the SEC actuator.

There is no requirement for the slip clutch for the SEC actuator. This is partly because the load configuration makes it difficult to backdrive the actuator during test, and partly because the low gear ratio makes it most unlikely that the motor can be back-driven at a damagingly high speed.

E. Scan Platform Settling Time

1. General. The settling time of the scan platform after a commanded slew is a critical requirement in the scan control system dynamics. One source of the settling time requirement, and apparently the most critical, is the resolution requirement of the television cameras that are mounted on the scan platform. In various phases of orbital flight, the

television cameras, together with other science instruments on the scan platform, will be slewed in the preprogrammed increments and sequences. The slew axes, the slew sequence, and the magnitude of slew angle vary depending upon the strategy of television picture forming during a given orbital flight. At the end of each slewing, after allowing some settling time for the scan platform, a television picture is taken. To obtain clear TV imaging, the TV shutter must be activated after the platform transient has subsided to an acceptable level. Therefore, the scan platform settling characteristics determine how soon a TV picture can be taken after each slewing and thus affect the TV imaging strategy in orbital flights.

2. Settling Time Requirement. It is assumed that the TV camera has a field of view (FOV) of 1.2 deg $\times$ 1.2 deg. Each view angle contains 1152 imaging dots or pixels; thus the entire FOV of the TV camera contains 1152 $\times$ 1152 pixels. The angle subtended by a pair of pixels in each view angle is 1.2 deg/1152 or about 0.001 deg (1.8×10^{-5} rad). To establish a criteria for the platform settling time from the TV imaging point of view, the following assumptions were made for the purpose of this analysis.

(1) If the peak-to-peak magnitude of the platform oscillation is limited to 1/2-pixel angle, there will be no overlaps of pixels; thus it is still possible to extract a meaningful set of imaging information.

(2) If the peak magnitude of angular movement is larger than 1/2-pixel angle, the maximum rate of angular motion must be limited to a value compatible with the maximum shutter exposure time being used to avoid overlaps of pixels. This relation can be expressed by:

$$\omega = \frac{\theta}{t} \tag{1}$$

where

θ = 1/2-pixel angle

t = shutter exposure time

(3) The angular rate can be larger than a value determined by the relation of Eq. (1) if the peak-to-peak amplitude of oscillation is less than 1/2 pixel.

According to the first assumption, the 1/2-pixel angle can be found as

$$\theta = \frac{1.2 \text{ deg}}{1152 \times 2} = 5.2 \times 10^{-4} \text{ deg } (9.1 \times 10^{-6} \text{ rad})$$

According to the second assumption, the maximum allowable rate when the oscillation amplitude exceeds 1/2-pixel angle can be found as

$$\omega = \frac{9.1 \times 10^{-6} \text{ rad}}{70 \times 10^{-3} \text{ s}} = 130 \times 10^{-6} \text{ rad/s}$$

where the maximum exposure time of 70×10^{-3} s was assumed. From the point of view of the scan platform maneuver and the TV picture taking sequencing, a set of settling time requirements is imposed on the scan control system. This requirement is tabulated in Table 3. As it is shown, the required settling time varies from 4 s for slew angles of 0.25 deg through 12 deg to a maximum of 20 s for angles greater than 60 deg. Since the scan control system employs a stepper-motor actuator, which drives the load at a constant speed and exhibits an identical start/stop transient characteristics regardless of the magnitude of the slew angle (unlike the linear position servo system), the worst case settling time requirement is 4 s. Therefore, this maximum settling time of 4 s applies to all slew angles.

3. Mathematical Model. To investigate the dynamic settling characteristics of the scan platform structure, a simplified dynamic model of the combined actuator/platform was constructed. This model, shown in Fig. 35, is a damped-inertia spring system. The estimated structural parameter values for the model are listed in Table 16. As shown in Table 16, there are two sources of mechanical damping torques. One damping torque is provided by the platform bearing friction T_f and has an estimated minimum value

of 0. 57 N-m; the other damping torque is provided by the viscous friction B and has a comparatively small value of 5. 4 N-m/(rad/s). The estimated value of the platform spring constant, which includes the actuator/platform linkage stiffness, is 6.5×10^3 N-m/rad.

Since the stepper motor is driven at a constant step rate during a commanded slew, the actuator output shaft essentially generates a ramp input, averaging about 1 deg/s to the scan platform structure. This ramp input causes the start/step transients to the platform structure. The linear and nonlinear torques described will tend to dampen the transients and aid to shorten the settling time.

To assess the effectiveness of the linear damping torque on the platform settling time, a linear model was constructed by neglecting the bearing friction and gear backlash.

The resulting transfer function is the second order system,

$$\frac{\theta_p(S)}{\theta_a(S)} = \frac{\frac{K}{J}}{S^2 + \frac{B}{J}S + \frac{K}{J}} = \frac{\omega_n^2}{S^2 + 2\xi\omega_n S + \omega_n^2}$$

where ω_n and ξ are the undamped natural frequency and the damping ratio, respectively. When the parameter values in Table 16 are substituted, ω_n and ξ are found as,

$$\omega_n = \sqrt{\frac{K}{J}} = 13.6 \text{ rad/s}$$

$$\xi = \frac{B}{2J\omega_n} = 0.01$$

As the low value of ξ indicates, no effective damping torque is provided by the viscous torque coefficient B.

When a step rate input is applied to the second order system and the inverse Laplace transformation is performed, the time domain solution of the output becomes,

$$\theta_p(t) = k\left[t - \frac{2\xi}{\omega_n} + \frac{1}{\omega_d}\exp(-\xi\omega_n t)\sin(\omega_d t - \psi)\right]$$

where:

$\psi = 2\tan^{-1}\omega_d/\xi\omega_n$

k = input rate

ω_d = damped natural frequency

The first term represents a linear position change with time; the second and third terms represent the initial offset and the transient terms, respectively. The transient term is, therefore, an exponentially damped sinusoid given by

$$\theta_p(t)_t = \frac{k}{\omega_d}\exp(-\xi\omega t)\sin(\omega_d t - \psi)$$

Using an exponential decay envelope to describe the system transient settling behavior, some system parameter values necessary in meeting the settling time requirement were estimated. This estimation assumes the absence of friction in the platform bearings. Assuming a design goal for a maximum settling time to be 2.5 s and using the exponential decay characteristics,

$$A = \frac{k}{\omega_d}\exp(-\xi\omega_n t)$$

where

$k = 1.75 \times 10^{-2}$ rad/s

$\omega_d \simeq \omega_n$

$A = 4.5 \times 10^{-6}$ rad (1/2-pixel width)

yields

$$\xi = 0.17$$

The linear damping coefficient B and the spring constant K required are:

$$B = 2\xi\omega_n J = 91.8 \text{ N-m/(rad/s)}$$

and

$$K = \omega_n^2 J = 3.8 \times 10^3 \text{ N-m/(rad)}$$

As the linear analysis indicates, the settling time can be reduced by increasing the combined spring constant of the actuator and the platform, and the structural viscous damping coefficient. Although the estimated value of the spring constant that appears in Table 15 is about the minimum required value, the calculated minimum value of the damping coefficient is about 29 times the estimated value. Computer simulation of the system response shows, however, that an effective damping can be provided by preloading the bearing friction in the platform gimbals.

4. Simulation Results. When the platform structure is subjected to a finite ramp input, two transients are generated: the initial transient that occurs when the ramp input is applied, and the final transient that occurs when the ramp is terminated. Thus, the two transients can combine into either an in-phase oscillation that results in a larger oscillation amplitude, or an out-of-phase oscillation that results in a smaller amplitude. A slew angle of 0.25 deg, for example, represents the first case as shown in Fig. 36. The damped natural frequency ω_d will be close in value to the natural frequency ω_n when the damping ratio ξ is small. Therefore, ω_d will be about 14 rad/s with the oscillation period of 0.45 s. The slew angle of 0.25 deg at 1 deg/s represents about a half period of oscillation; thus, the two transients $\theta(t)u(t_1)$ and $-\theta(t)u(t_1 - 0.25)$ are in-phase oscillations that yield a larger resultant amplitude. Similarly, a slew angle of 0.5 deg, for example, will produce out-of-phase oscillations that yield a small resultant amplitude. The above examples show that the transient settling time of the platform varies depending not only on the structural parameters but also on the magnitude of the slew angle.

Since the linear analysis was utilized for the primary assessment of the platform structural behavior, some nonlinear effects that exist in the actual

system were neglected. Some of those effects neglected in the analysis were the effects of the platform bearing friction and the actuator gear backlash on the platform settling characteristics. These effects were included in the digital computer simulation of a simplified platform model. Figure 37 shows a block diagram of the simulated platform model. In the simulation runs, the assumed bearing friction T_f of 0.57, 1.1, and 1.7 N-m were used to investigate the variations in the settling characteristics of the platform, and the results are summarized in Table 17. As shown in Table 17, the settling time decreases in inverse proportion to the friction torque values, and the settling time of less than 1 s occurs with a T_f of 1.1 N-m. The settling time, as described previously, is the time that the peak-to-peak amplitude of oscillation of the platform decays to 9.1×10^{-6} rad after the completion of the slew, or the time that the peak rate of oscillation is reduced to 130×10^{-6} rad/s. The actual settling time estimated from the computer simulation is the time that the major oscillation ceases and the platform comes to a stop. Figure 38 shows the settling characteristics for a slew angle of 0.25 deg at a slew rate of 1 deg/s. Figure 38(a) shows the case for a total bearing friction of 0.57 N-m and with absence of gear backlash.

Figure 38(b) shows a case similar to Fig. 38(a) except a backlash of ±0.035 deg was added. It is seen that the gear backlash has an effect of damping the transient response, thus reducing the settling time. The settling time is shown to be about 1.5 s. Figures 38(c) and (d) show cases similar to Figure 38(b) except the bearing friction was increased to 1.1 N-m and 1.7 N-m, respectively. As a result, the settling time has decreased to about 0.75 s and 0.5 s, respectively. Figure 38(e) shows a case similar to Fig. 38(c) except the slew angle was doubled to 0.5 deg. Note the change in the settling characteristics due to the difference in the slew angles.

F. Breadboard Test Results

Some test results were obtained using the ARTC breadboard shown in Fig. 39. The breadboard consists of Channel A and Channel B control electronics and four breadboard actuators. The actuator breadboard represents two axes of scan actuators and two axes of SEC actuators.

Table 18 contains data taken at 25°C. The breadboard used randomly selected electronic parts, and was tested with no adjustments. The breadboard was operated in closed loop and commanded to a position by a simulated CCS CC.

The subsystem electronics error was determined by measuring the electrical displacement of the feedback potentiometer by use of a four-digit ratiometer and, therefore, errors due to potentiometer imperfections are not included. Similar data was taken at intervals from -25°C to +85°C, and is displayed in the graphs of Fig. 40. These are plots of the position error vs commanded position for a range equivalent to the scan clock axis and show that the error over the temperature range is smaller than half the least significant bit of 0.125 deg. The test data includes some errors that were not accounted for in the static error analysis shown in Table 10. The noise voltages at the input to the comparator can introduce an error by causing a premature zero-crossing detection. The noise filter in the feedback loop produces phase shift into the feedback signal causing a delay in the zero-crossing detection. The digital actuator provides the feedback signal in discrete steps and can cause an error of as much as one full step after zero-crossing. Also there is hysteresis associated with the comparator that will introduce a fixed position error. There are measurement errors caused by the limited resolution of the ratiometer used in the test. The errors introduced by the actuator step size and the comparator hysteresis are estimated to be about 0.01 deg and 0.015 deg, respectively. The errors associated with the ratiometer resolution is estimated to be about ±0.013 deg.

G. Subsystem Errors

The pointing and positioning accuracies of the scan, HGA, and SEC control loops are specified in Table 3. To assess the total ARTC error contribution to the spacecraft system pointing errors, the errors in the ARTC control loops have been estimated and listed in Tables 19 and 20. The error specified in Table 3 represents the sum of the errors from the ARTC with respect to the spacecraft-fixed coordinate axes and the errors in pointing of the spacecraft in space with respect to the space-fixed coordinate axes. The spacecraft pointing errors include those from limit cycle operations of the Attitude Control Subsystem and misalignments of the navigational sensors. Tables 19 and 20 list only those errors generated in the ARTC.

Table 19 shows estimated errors in the scan cone axis. For the scan clock axis, each error component is multiplied by the sine of the cone angle since the angular movement in the clock axis is geometrically related to the cross-cone axis by the sine of the cone angle. The errors due to the control

electronics were taken from the results in Table 10. The errors related to the feedback potentiometer, namely the potentiometer calibration errors and the step-size errors due to potentiometer nonlinearity, were estimated from the result of a preliminary investigation of the potentiometer characteristics. The hysteresis in the platform structure and the actuator represent an estimated maximum value and a specified maximum value, respectively. Table 20 shows a summary of estimated control errors for the HGA and SEC control loops. The control error for the SEC represents the sum of the errors about the commanded position. For the positioning error the input step size must be included in the computation. Although the input step size currently planned for the SEC is an equivalent of a 6-bit resolution (1.43 deg), the step size as fine as an equivalent of a 9-bit resolution (0.18 deg) is available. The choice of input step size will be dependent largely upon the temperature control requirements.

H. Production Proof Model

Since the writing of the material in this report, the preproduction model (PPM) of the Articulation Control Subsystem electronics assembly has been built and it is being tested. The photographs of the PPM are shown in Fig. 41. The package measures approximately $38.2 \times 3.82 \times 16.8$ cm.

Table 1. Functional requirements

Control axes	Command step size, deg	Operate range, deg	Slew rate, deg/s	
			High	Low
Scan clock	0.25	230	1.0	0.25
Scan cone	0.25	130	1.0	0.25
HGA, az	0.20	181	1.0	0.25
HGA, el	0.20	200	1.0	0.25
SEC 4	1.50	90	13.6	3.4
SEC 6	1.50	90	13.6	3.4
SEC 12	1.50	90	13.6	3.4
SEC 14	1.50	90	13.6	3.4

Table 2. System error tolerance requirements

Output	Control, deg	Knowledge, deg
Scan	±0.5[a]	±0.25[a]
HGA	±0.7[a]	-
SEC	±1.0	-

[a]Applies to spacecraft systems.

Table 3. Scan platform settling time requirements

Slew angle, deg	Settling time, s
0 to 12	4.0
12 to 60	1/3 of slew time
>60	20.0

Table 4. ARTC telemetry outputs

Signal location	Telemetry channel names
Scan clock actuator	TLM scan clock position coarse
	TLM scan clock position fine
Scan cone actuator	TLM scan cone position coarse
	TLM scan cone position fine
HGA elevation actuator	TLM HGA elevation position coarse
	TLM HGA elevation position fine
HGA azimuth actuator	TLM HGA azimuth position coarse
	TLM HGA azimuth position fine
SEC actuators	TLM SEC 4 position
	TLM SEC 6 position
	TLM SEC 12 position
	TLM SEC 16 position

Table 5. CCS CC to ARTC

Symbol	Name	Destination	Comment
15E	Scan clock position	ARTC 1[a]	Sets clock angle reference.
15F	Scan clock position	ARTC 2[b]	
15G	Scan cone position	ARTC 1	Sets cone angle reference.
15H	Scan cone position	ARTC 2	
15J	HGA az position	ARTC 1	Sets azimuth angle reference.
15K	HGA az position	ARTC 2	
15L	HGA el position	ARTC 1	Sets elevation angle reference.
15M	HGA el position	ARTC 2	
15N	SEC 4 position	ARTC 1	Sets SEC 4 blade angle reference.
15P	SEC 4 position	ARTC 2	
15Q	SEC 6 position	ARTC 1	Sets SEC 6 blade angle reference.
15R	SEC 6 position	ARTC 2	
15S	SEC 12 position	ARTC 1	Sets SEC 12 blade angle reference.
15T	SEC 12 position	ARTC 2	

[a] ARTC 1 = channel A.

[b] ARTC 2 = channel B.

Table 5. CCS CC to ARTC (contd)

Symbol	Name	Destination	Comment
15U	SEC 14 position	ARTC 1	Sets SEC 14 blade angle reference.
15V	SEC 14 position	ARTC 2	
15W	High-rate slew	ARTC 1	1.0 deg/s for scan and HGA. 13.8 deg/s for SECs
15WR	Low-rate slew	ARTC 1	0.25 deg/s for scan and HGA. 3.45 deg/s for SECs
15Y	High-rate slew	ARTC 2	1.0 deg/s for scan and HGA. 13.8 deg/s for SECs
15YR	Low-rate slew	ARTC 2	0.25 deg/s for scan and HGA. 3.45 deg/s for SECs

Table 6. CCS DC for ARTC functions

Symbol	Name	Destination (subsystem)	Comment
15A	ARTC 1 ON	PWR	Switches 2.4 kHz power to ARTC 1 electronics.
15AR	ARTC 1 OFF	PWR	Removes 2.4 kHz power from ARTC 1 electronics.
15B	ARTC 2 ON	PWR	Switches 2.4 kHz power to ARTC 2 electronics.
15BR	ARTC 2 OFF	PWR	Removes 2.4 kHz power from ARTC 2 electronics.
15C	Platform unlatch	PYRO	Releases the pressure from the scan platform latch.
15D	HGA unlatch	PYRO	Unlatches the high-gain antenna.

Table 7. ARTC output selection logic

Coding			Output
C	B	A	
1	1	1	Scan clock
0	1	1	Scan cone
1	0	1	Antenna azimuth
0	0	1	Antenna elevation
1	1	0	SEC 4
0	1	0	SEC 6
1	0	0	SEC 12
0	0	0	SEC 14

Table 8. High/low slew mode selection logic[a]

Output	Coding			LSB	Function
	C	B	A		
SEC 4	1	1	0	0	Position control
				1	High-rate slew mode
SEC 6	0	1	0	0	Position control
SEC 12	1	0	0	0	Position control
SEC 14	0	0	0	0	Position control
				1	Low-rate slew mode

[a]Refer to Fig. 4 for data word format.

Table 9. Timing values for signals in Fig. 19

Pulse width	High rate (100Hz)	Low rate (25Hz)
t4, μs	208	208
t5, ms	20	80
t6, μs	416	416
t7, ms	10	40
t8, ms	8	8

Table 10. Total errors contributed by ARTC electronics [a]

Error source	Error, mV	$(\text{Error})^2$, mV^2
Ratio match of DAC resistors	± 0.79	0.62
Ratio match of summing resistors	± 0.79	0.62
Ratio match of inverting amplifier gain setting resistors	± 0.79	0.62
Saturation resistance of DAC switches	± 1.63	2.65
Initial offset voltage of DAC inverting amplifier	± 1.5	2.25
Offset voltage drift of DAC inverting amplifier	± 0.45	0.202
Initial offset voltage of comparator	± 0.75	0.562
Offset voltage drift of comparator	± 0.45	0.202
Initial offset voltage of buffer amplifier	± 0.5	0.25
Offset voltage drift of buffer amplifier	± 0.3	0.09
Multiplexer switch leakage current	± 1.2	1.44
Total	9.18	9.57

[a] $\pm\sigma = 0.58\,(9.57)^{1/2} = 1.78$ mV

Full scale = 12.4 V

Table 11. Average dc power consumption for various operational modes

Mode	Stand-by	Slew	
		Scan	HGA/SEC
One channel, W	3.8	12.6	9.2
Two channel, W	7.6	25.2	18.4

Table 12. System scale factors and telemetry resolution

Parameter	Scan		HGA		SEC,
	Coarse	Fine	Coarse	Fine	coarse
Telemetry resolution, deg/DN[a]	2.0	0.04	1.6	0.05	0.7
Feedback pot scale factor, mV/deg	48.2		60.6		135.2

[a]DN = data number

Table 13. Motor winding grounding sequence

Direction	Sequence			
	1	2	3	4
CCW	W1	W2	W3	W4
CW	W1	W4	W3	W2

Table 14. Stepper motor characteristics for scan actuator

Characteristic	Size 11	Size 15
Motor output torque,[a] N-m	3×10^{-3}	8.5×10^{-3}
Actuator output torque,[a, b] N-m	18.6	53.4
Power input, W	7.8	13.1
Weight, g	85.0	255.0
Motor detent torque, N-m	2.1×10^{-3}	5.3×10^{-3}
Actuator holding torque,[b] N-m	27.2	68.0

[a]At 100 steps/s rate.

[b]A gear ratio of 9000 and torque transmission efficiency of 0.7 assumed.

Table 15. Stepper motor characteristics for HGA and SEC actuators

Parameter	HGA	SEC
Motor output torque,[a] N-m	8.4×10^{-4}	8.4×10^{-4}
Actuator detent torque, N-m	5.3[b]	0.4
Power input, W	4.4	4.4
Actuator detent torque, N-m	9.1[b]	0.67

[a]At 100 steps/s rate.

[b]A gear ratio of 9000 and torque transmission efficiency of 0.7 assumed.

[c]A gear ratio of 660 and torque transmission efficiency of 0.7 assumed.

Table 16. Platform parameters

Symbol	Parameter	Estimated nominal value
K_a	Actuator spring constant	8.1×10^3 N-m/rad
K_p	Platform spring constant	6.5×10^3 N-m/rad
K	Combined spring constant	3.6×10^3 N-m/rad
J	Platform inertia	20.3 Kg-m^2
B	Viscous damping	5.4 N-m/rad/s
T_f	Platform bearing friction	0.57 N-m
Θ_a	Actuator position	-
Θ_p	Platform position	-

Table 17. Summary of simulation runs[a]

Total friction, N-m	Settling time, s
0.57	1.5
1.1	0.75
1.7	0.5

[a]Slew rate : 1 deg/s.
Backlash : $\pm 0.59 \times 10^{-3}$ rad.
Slew angle: 0.25 deg.

Table 18. System test data at +25°C

Input digital code	Input ideal ratio	Measured channel A output	Measured channel B output
1111111000	0.99267	0.9925	0.9927
1101111111	0.87451	0.8747	0.8743
1100000000	0.75049	0.7506	0.7503
1001111111	0.62451	0.6247	0.6242
1001000000	0.56298	0.5629	0.5628
1000011111	0.53076	0.5308	0.5306
1000000011	0.50342	0.5034	0.5033
0111111111	0.49951	0.4995	0.4994
0111100000	0.46923	0.4692	0.4693
0110111111	0.43701	0.4370	0.4369
0110000000	0.37549	0.3755	0.3755
0011111111	0.24951	0.2496	0.2495
0010000000	0.12549	0.1255	0.1255
0000000111	0.00732	0.0073	0.0072

Table 19. Scan pointing errors (cone axis)

Error source	Control, deg	Knowledge, deg
Electronics[a]	0.037	—
Potentiometer calibration[a]	—	0.05
Potentiometer nonlinearity	0.017[c]	—
Input step size[b]	0.125	—
Hysteresis, platform[b]	0.05	0.05
Hysteresis, actuator[b]	0.10	—
Step size, actuator[b]	0.01	—
Telemetry Resolution[b]	—	0.02
Total (3σ)	0.31	0.18

[a]Normal error distribution assumed (1-σ value).

[b]Uniform error distribution assumed (maximum value).

[c]After calibration.

Table 20. HGA and SEC control errors

Error source	HGA, deg	SEC, deg
Electronics[a]	0.029	0.013
Potentiometer nonlinearity	0.017[c]	0.18
Input step size[b]	0.10	—
Hysteresis, structure[b]	0.05	0.05
Hysteresis, actuator[b]	0.16	0.5
Step size, actuator[b]	0.01	0.136
Total (3σ)	0.36	0.95

[a]Normal error distribution assumed (1-σ value).

[b]Uniform error distribution assumed (maximum value).

[c]After calibration.

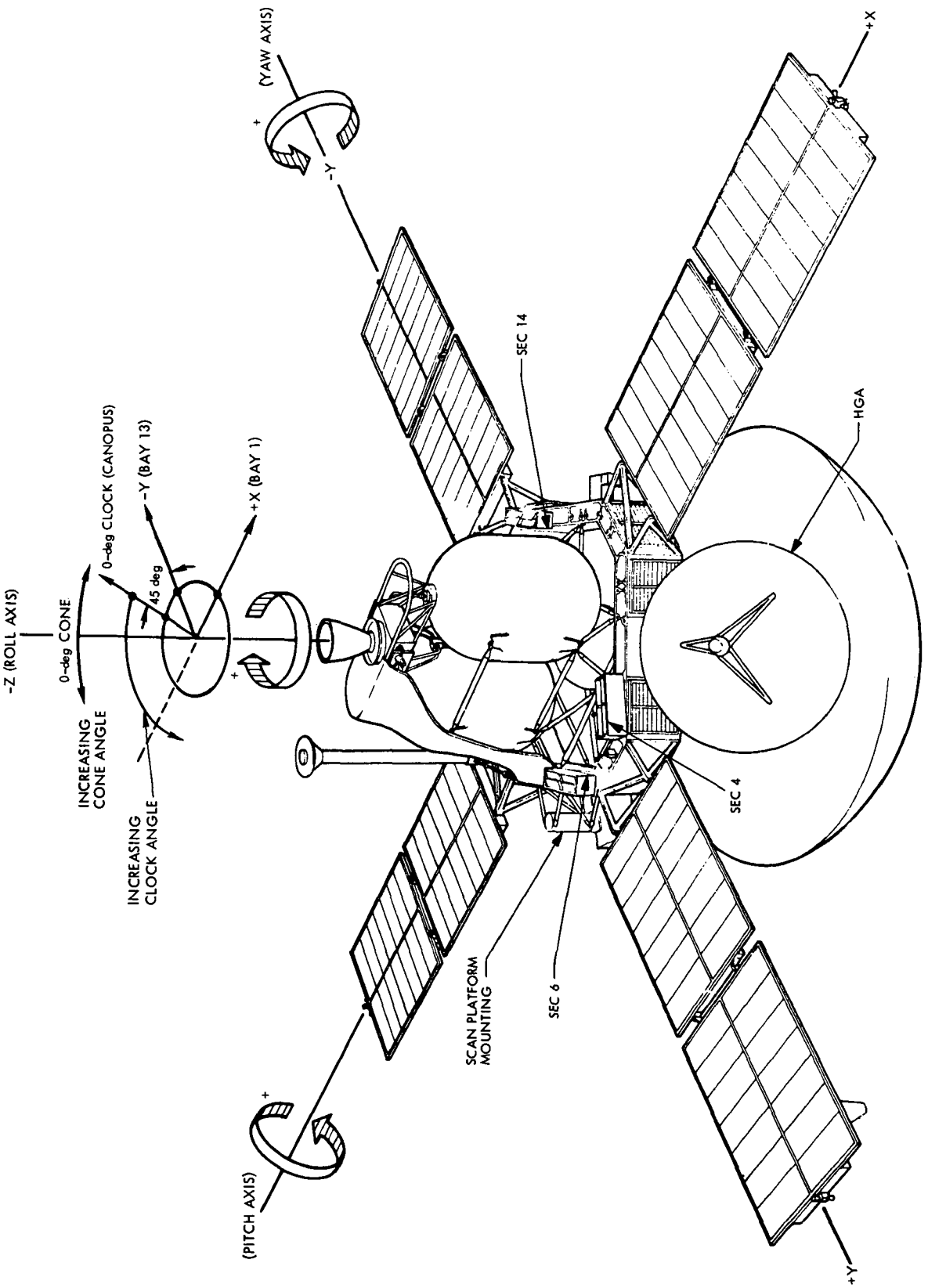

Fig. 1. Orbiter coordinate system

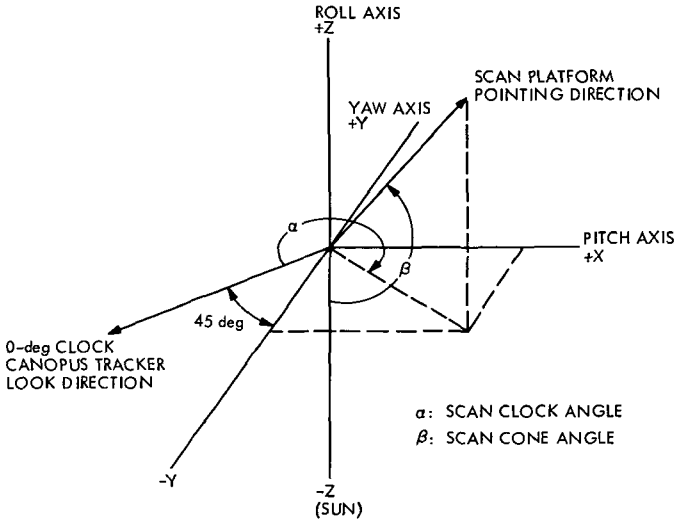

Fig. 2. Scan platform system coordinate convention

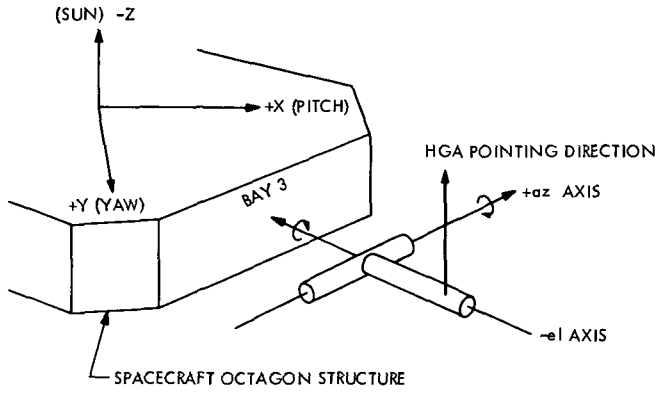

Fig. 3. HGA system coordinate convention

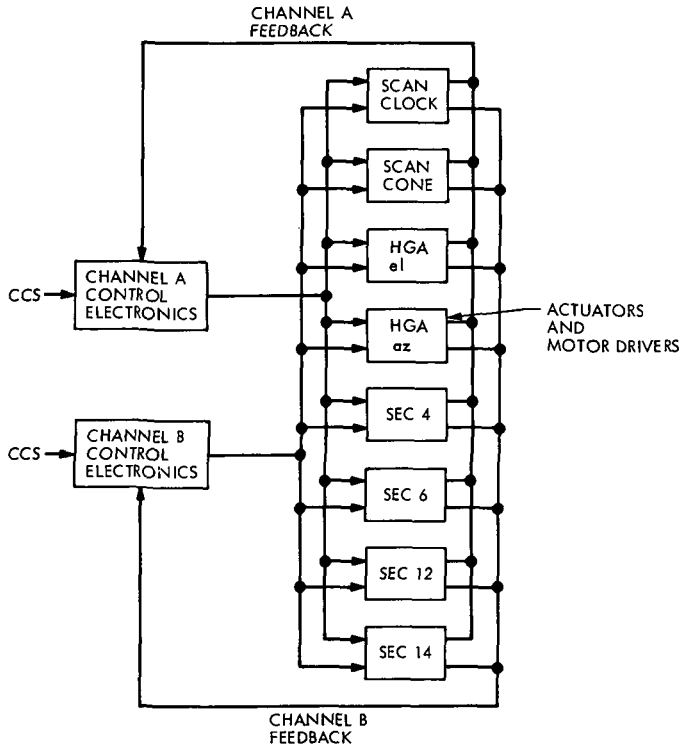

Fig. 4. Simplified ARTC block diagram

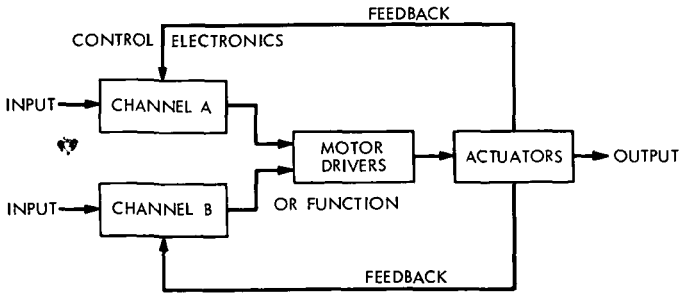

Fig. 5. Articulation control subsystem showing redundant control function

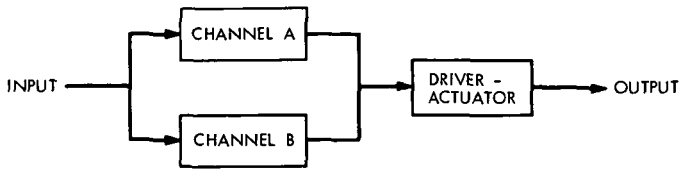

Fig. 6. Equivalent system representation

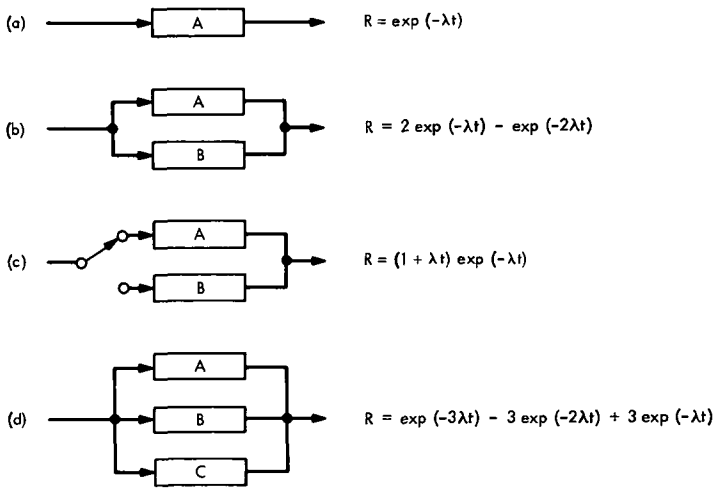

Fig. 7. Various redundancy schemes

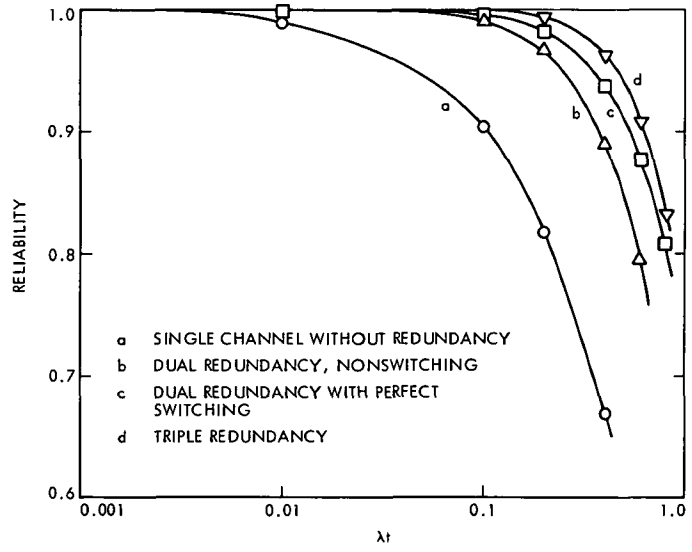

Fig. 8. Comparison of redundancy configurations

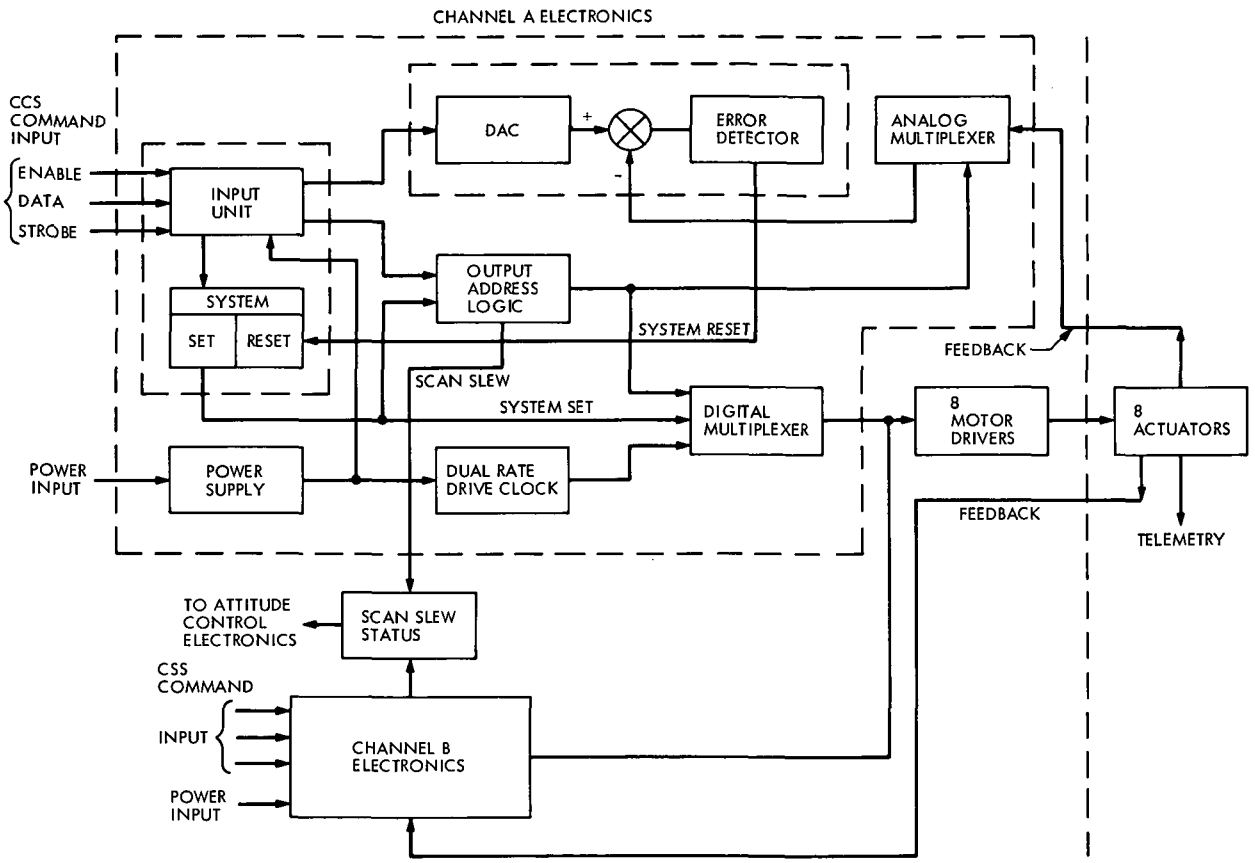

Fig. 9. ARTC subsystem electronics block diagram

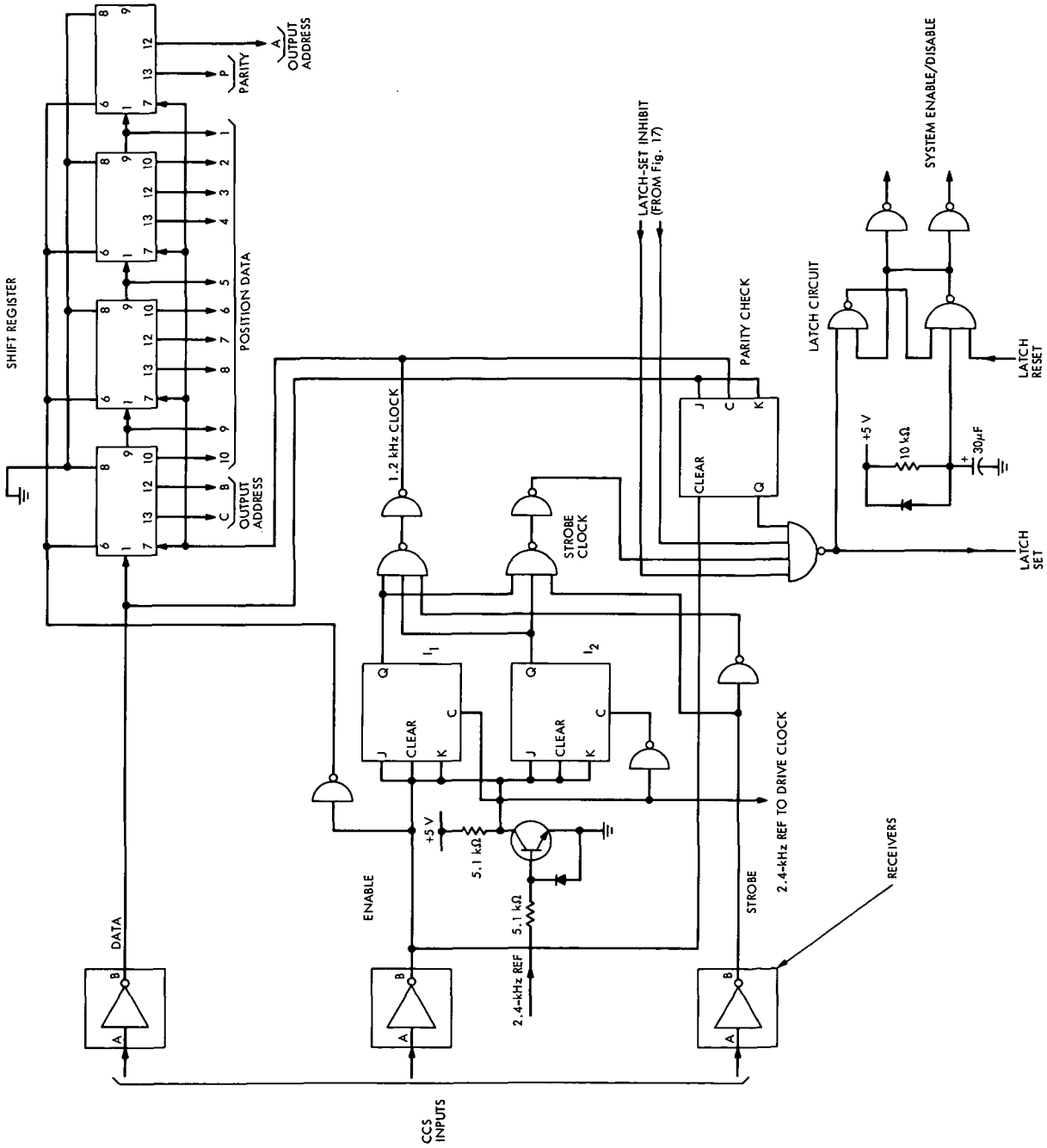

Fig. 10. Input unit

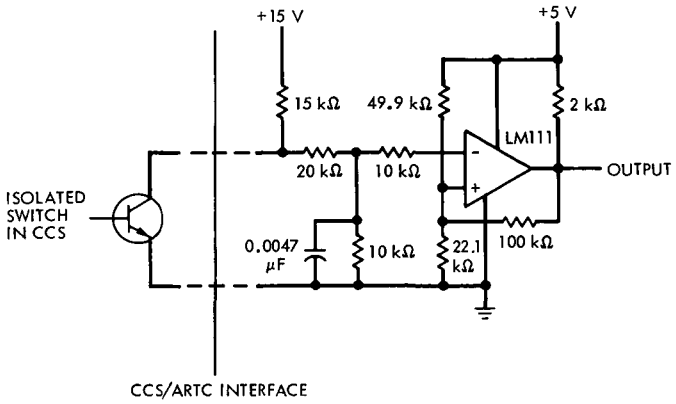

Fig. 11. Schematic diagram of ARTC input receiver

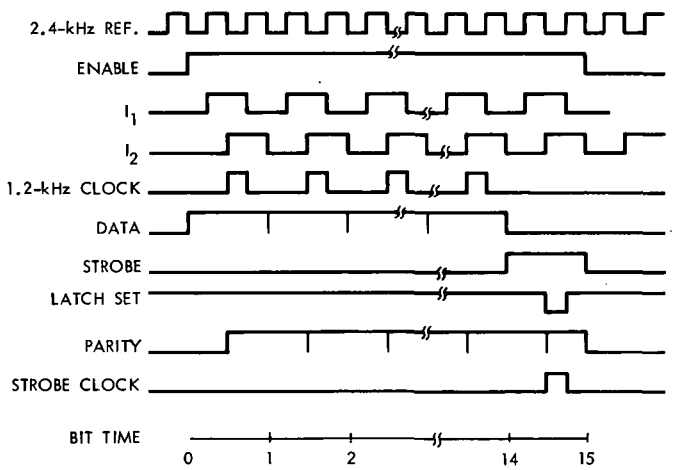

Fig. 12. Signal timing diagram

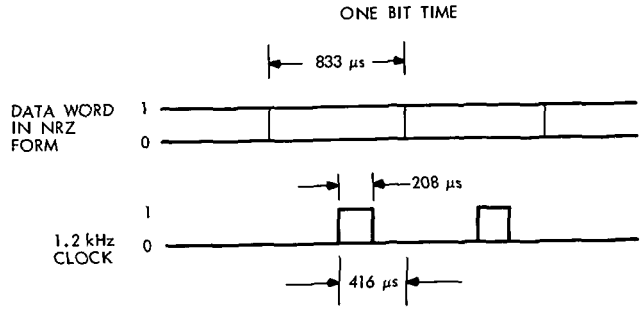

Fig. 13. Shift register clock position in the data field

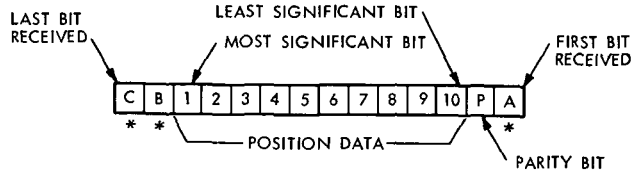

* OUTPUT SELECTION BIT, SEE TABLE 7

Fig. 14. CCS data format

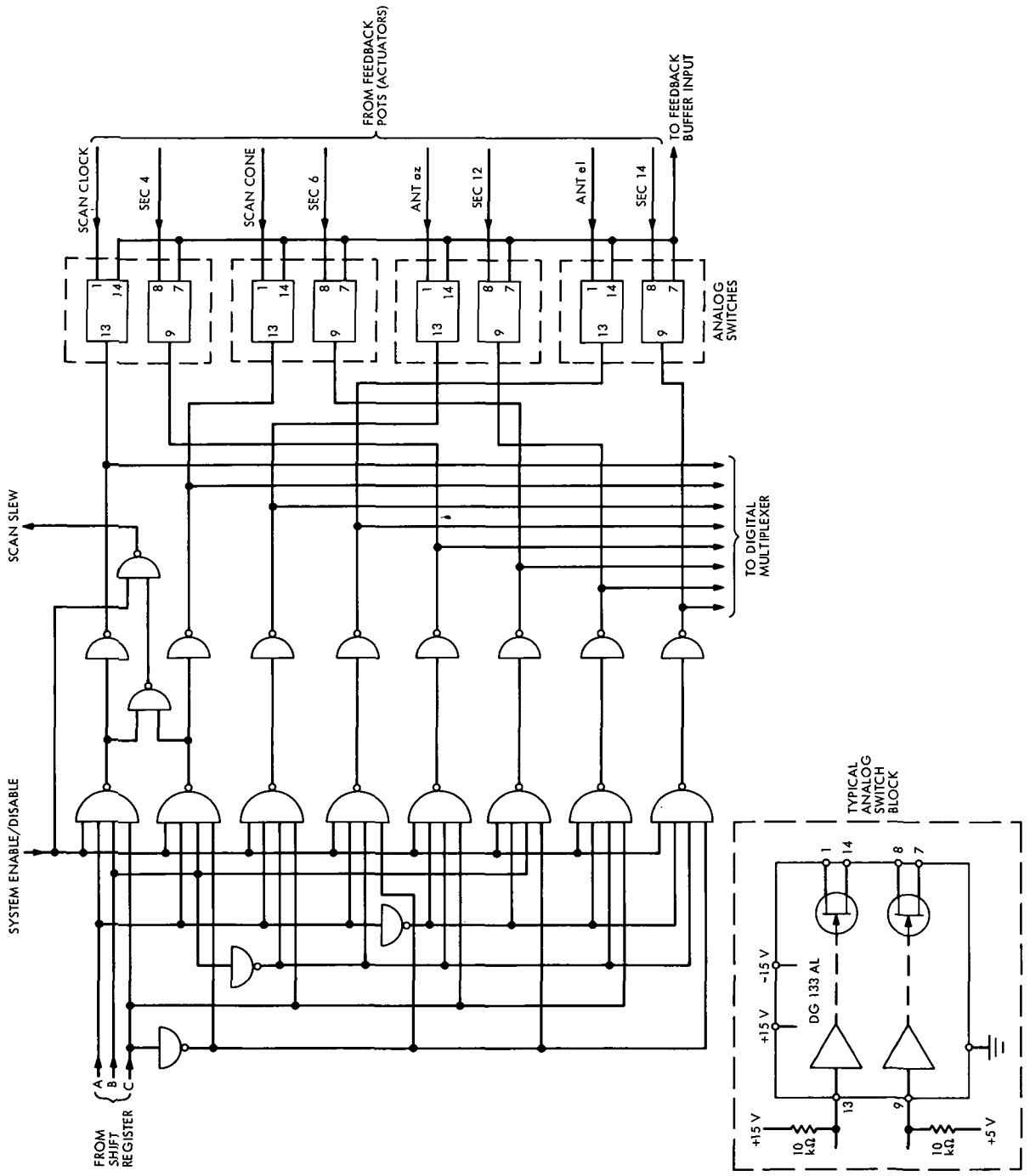

Fig. 15. Output selection logic and analog multiplexer

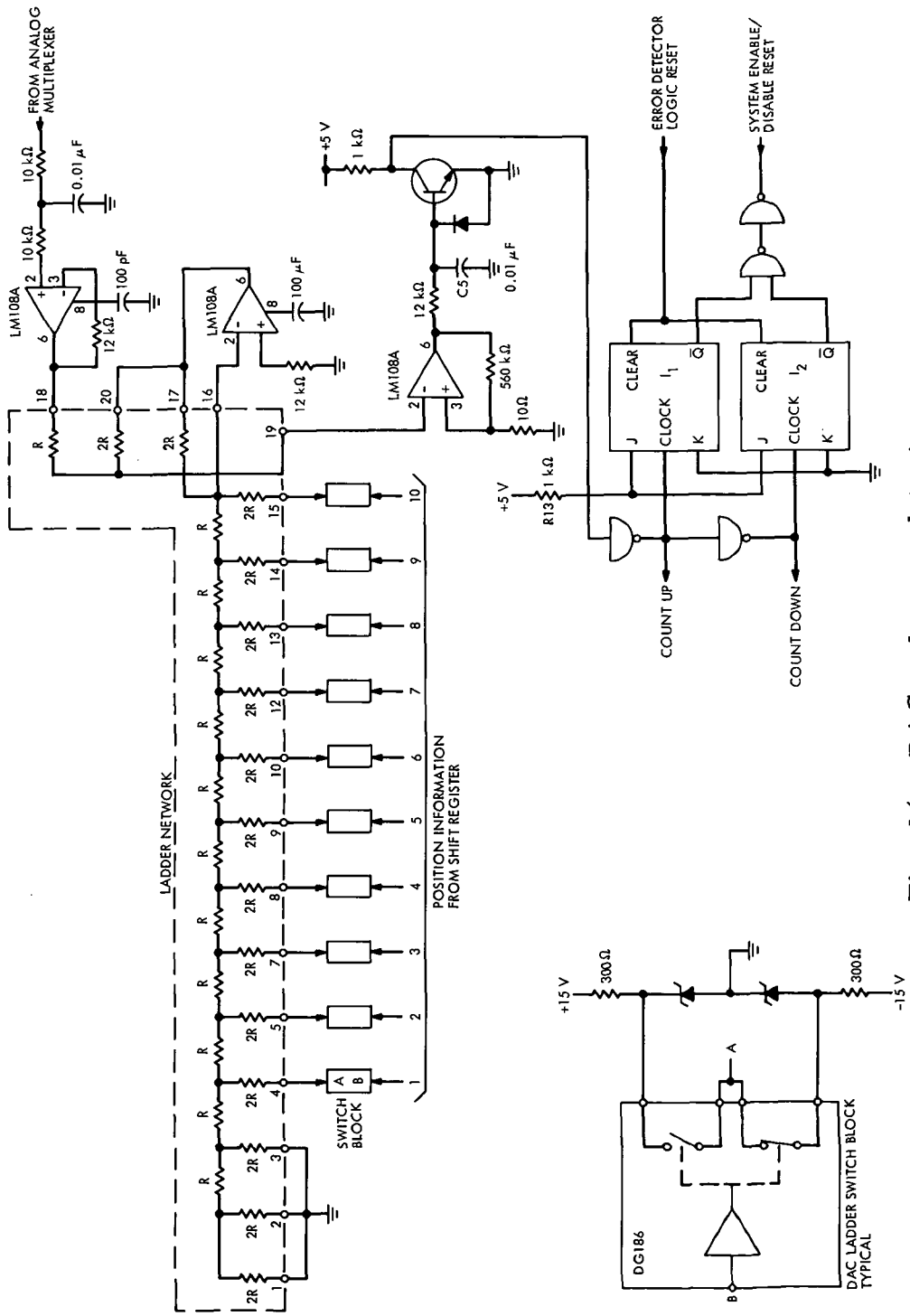

Fig. 16. DAC and error detector

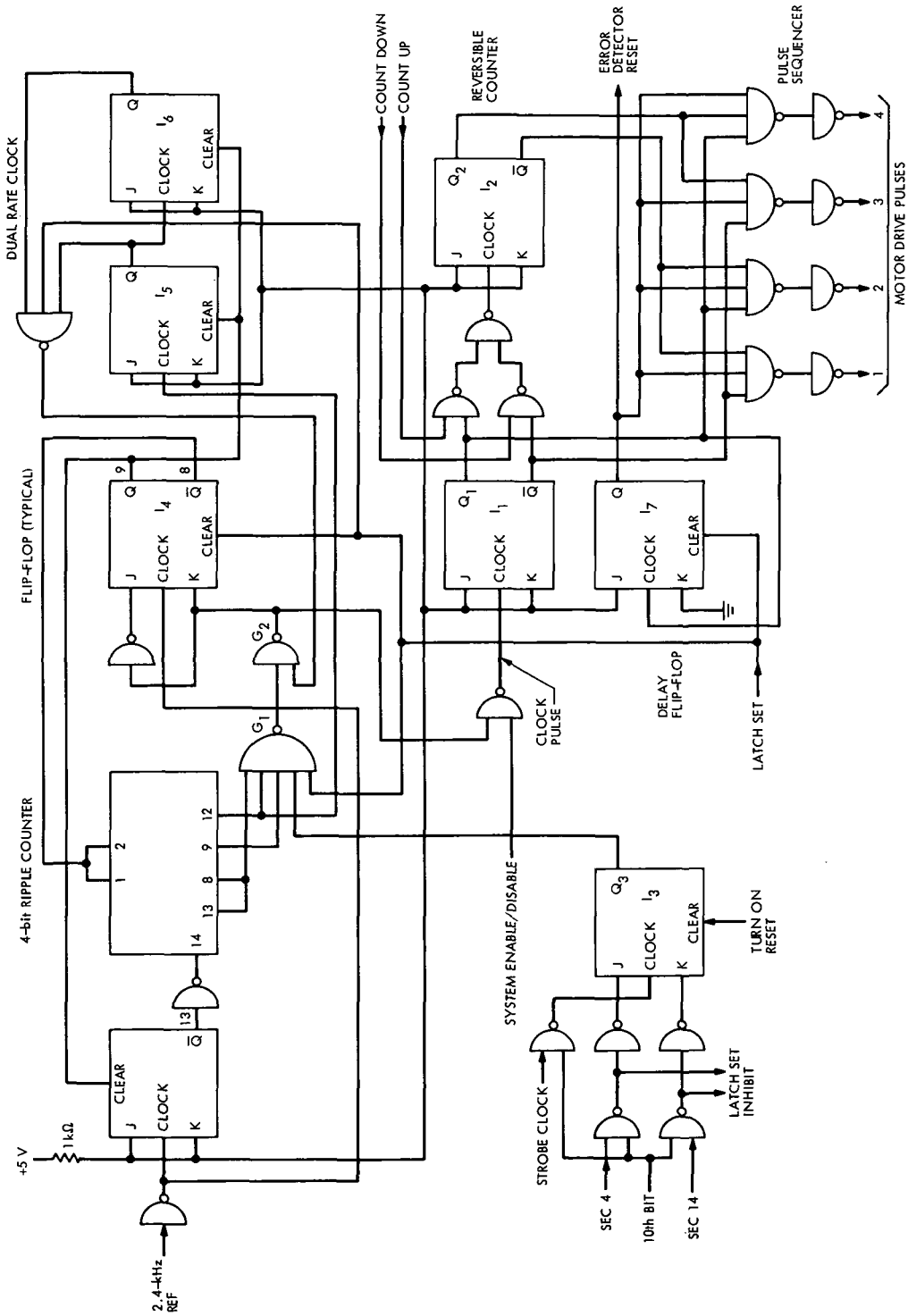

Fig. 17. Motor drive pulse generator

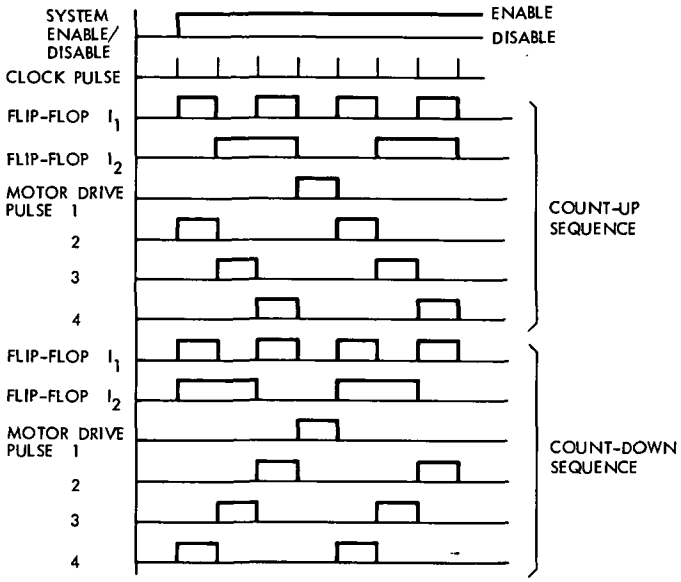

Fig. 18. Motor drive pulse sequencing

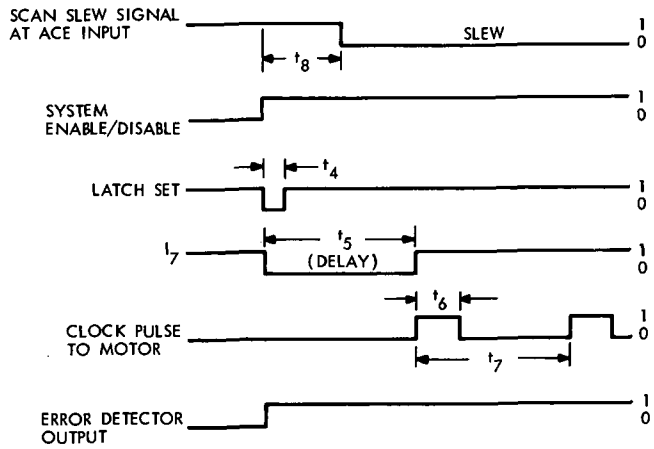

Fig. 19. Delayed clock pulses and scan slew following latch set signal

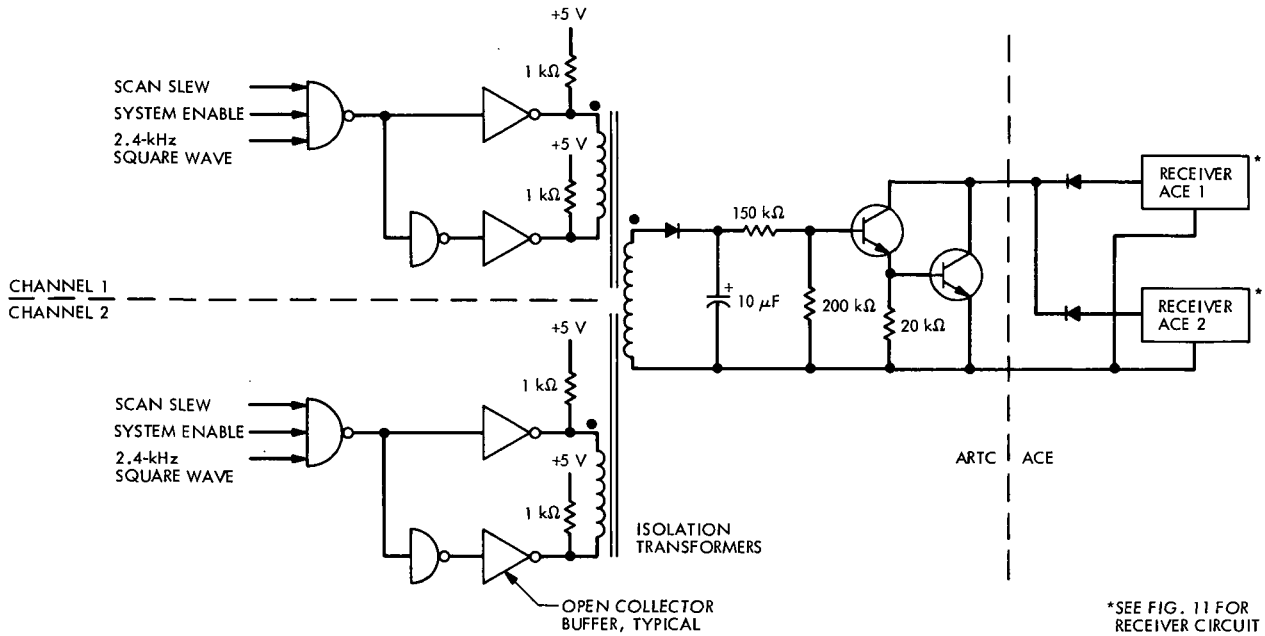

Fig. 20. ARTC/ACE interface circuit for scan slew signal

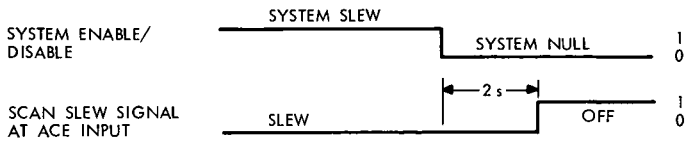

Fig. 21. Scan slew signal with a turn-off delay

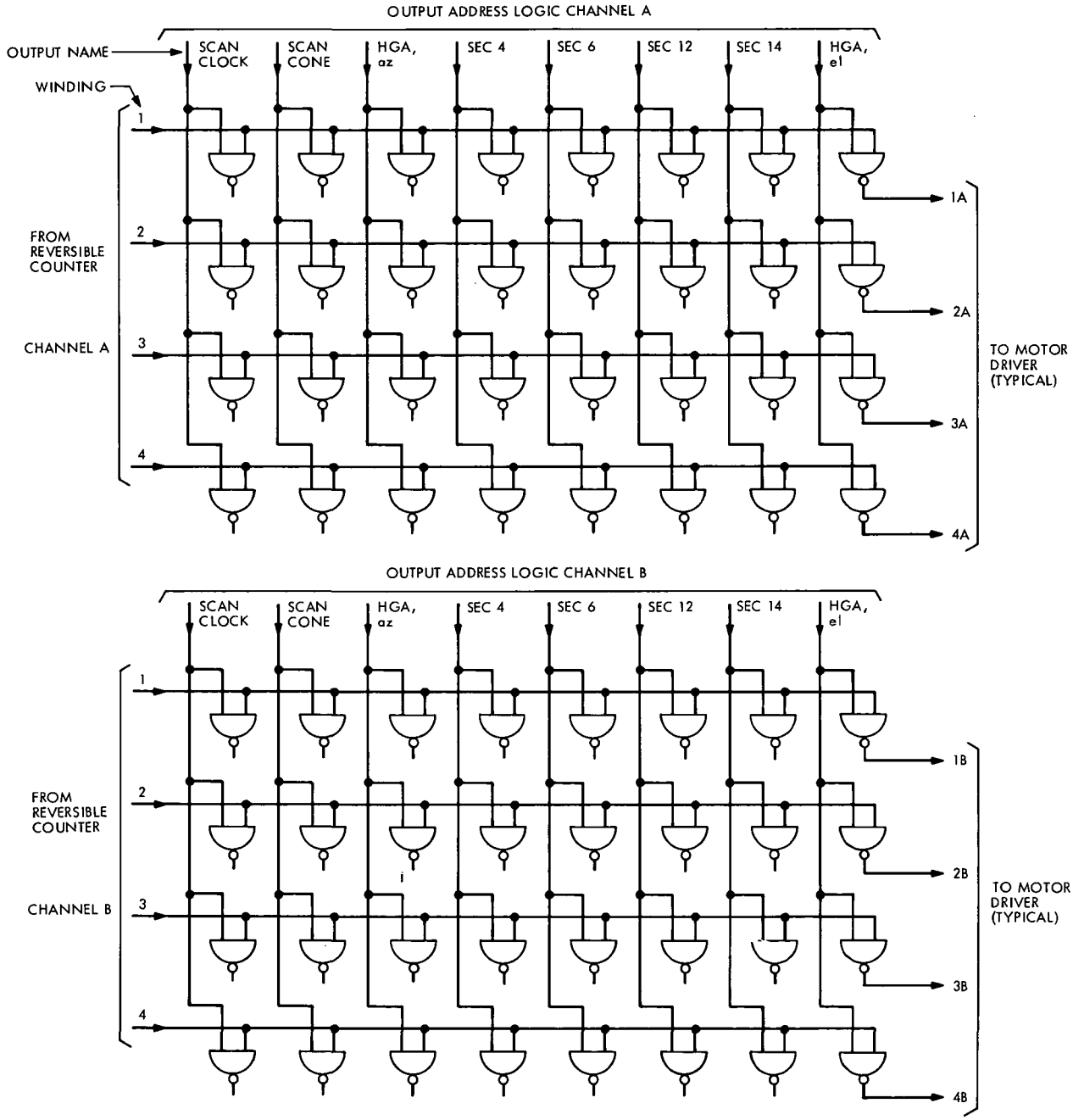

Fig. 22. Digital multiplexer

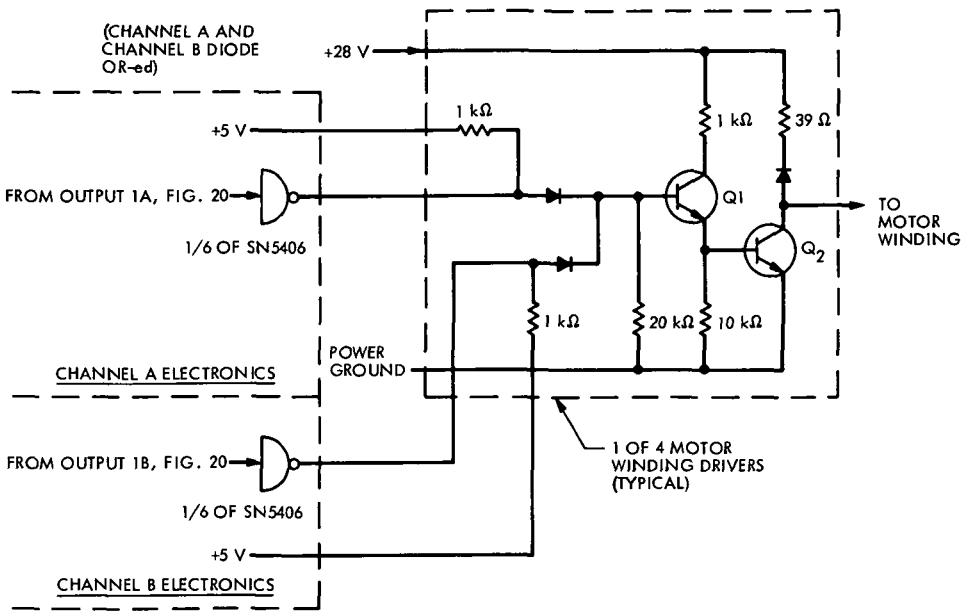

Fig. 23. Typical motor driver circuits and channel OR-ing scheme

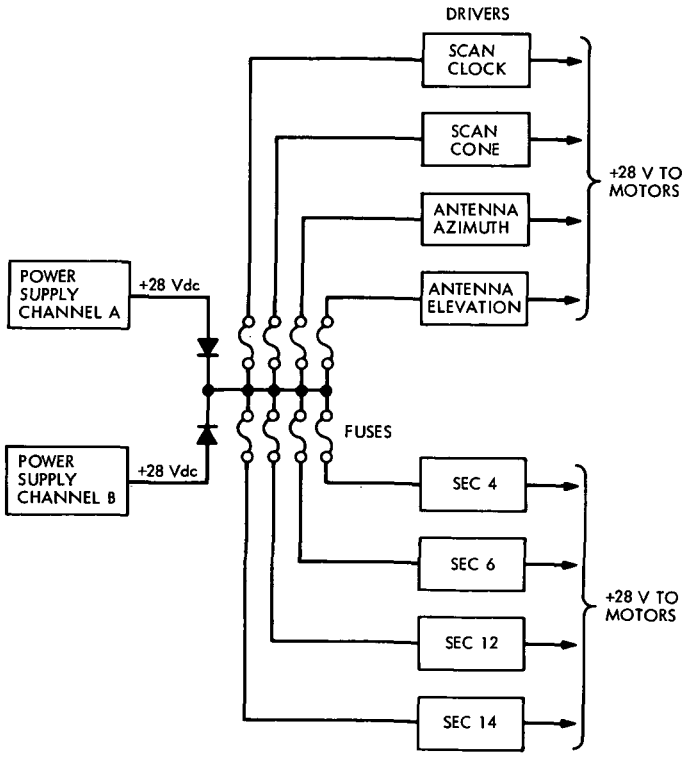

Fig. 24. Driver power distribution configuration

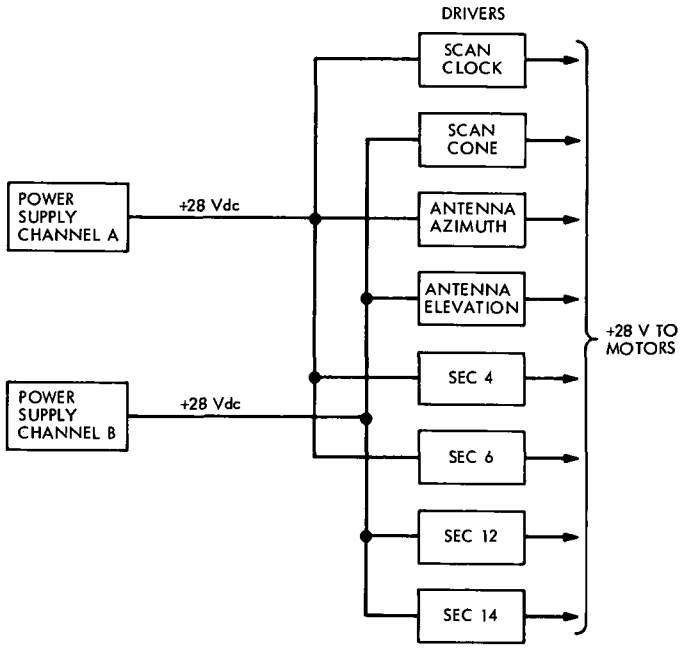

Fig. 25. Alternate driver power distribution configuration

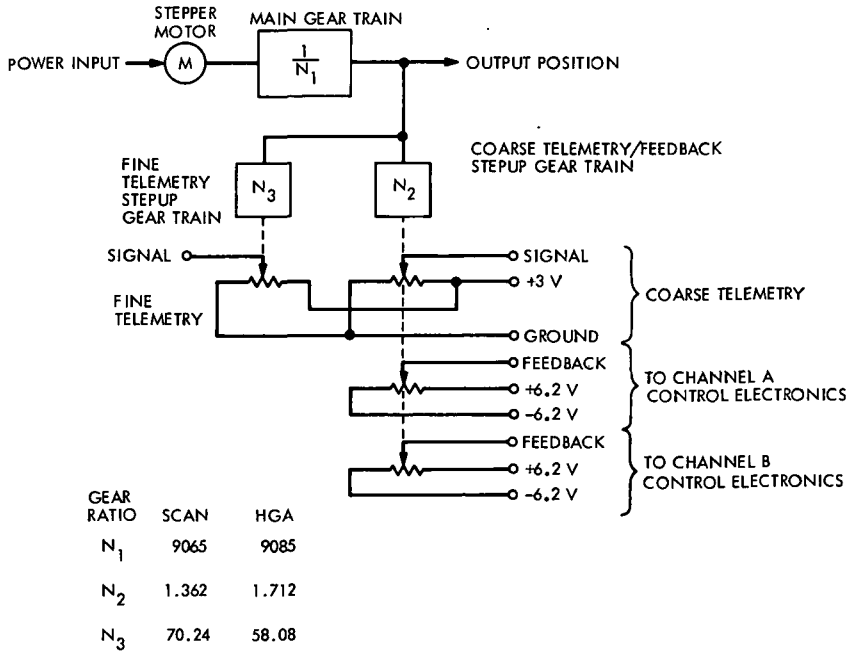

GEAR RATIO	SCAN	HGA
N_1	9065	9085
N_2	1.362	1.712
N_3	70.24	58.08

Fig. 26. Schematic diagram of scan and HGA actuator

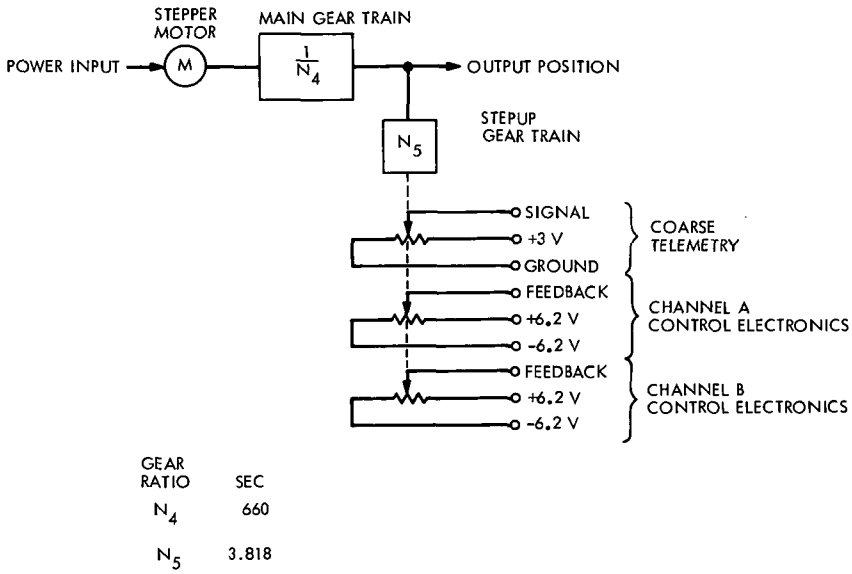

Fig. 27. Schematic diagram of SEC actuator

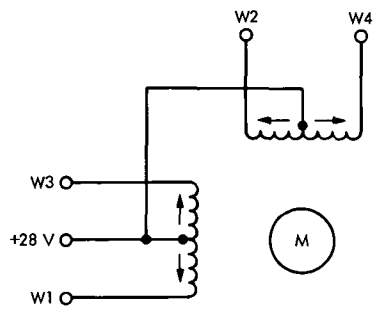

Fig. 28. Stepper motor schematic diagram

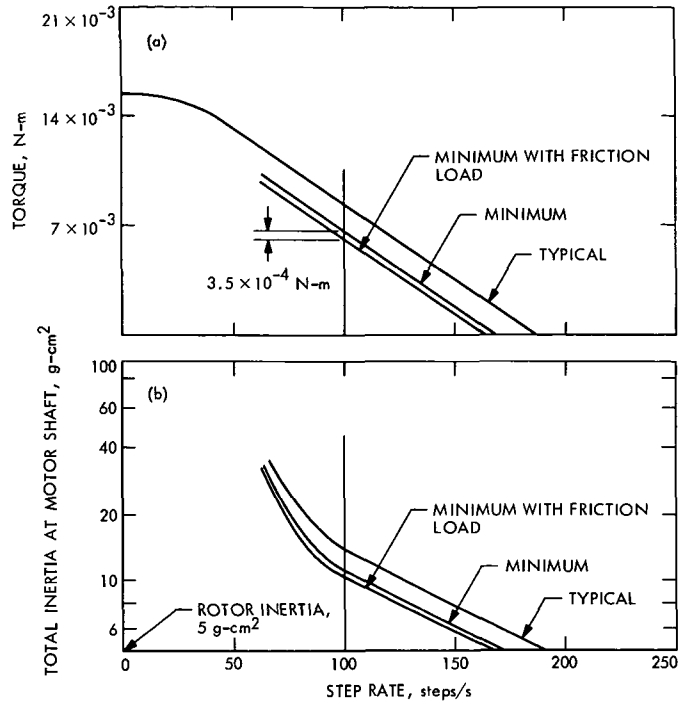

Fig. 29. Size 15 stepper motor characteristics

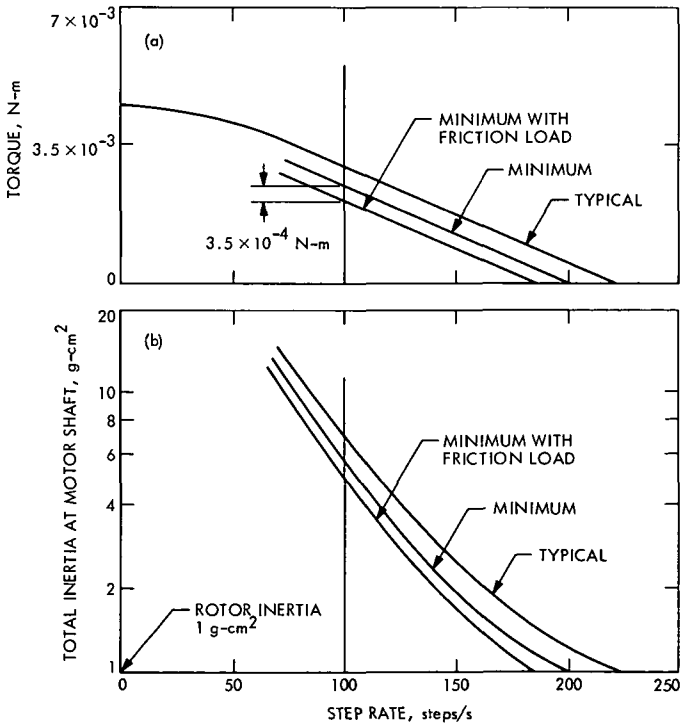

Fig. 30. Size 11 stepper motor characteristics

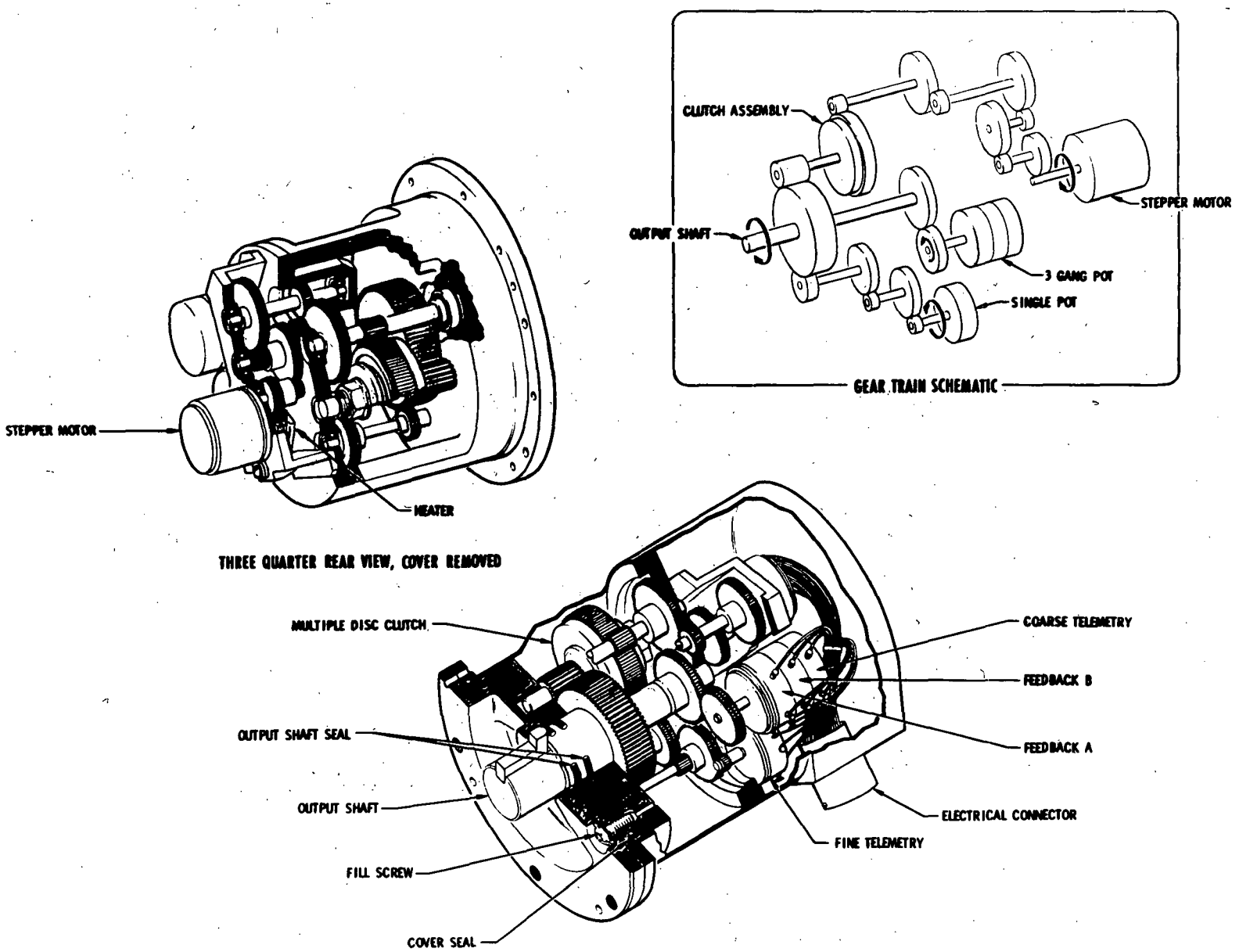

Fig. 31. VO75 scan actuator

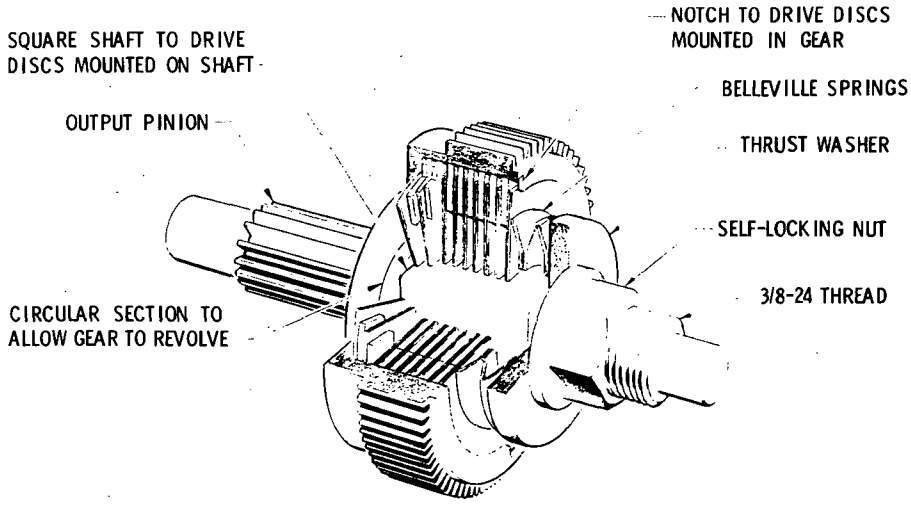

Fig. 32. Clutch assembly scan actuator

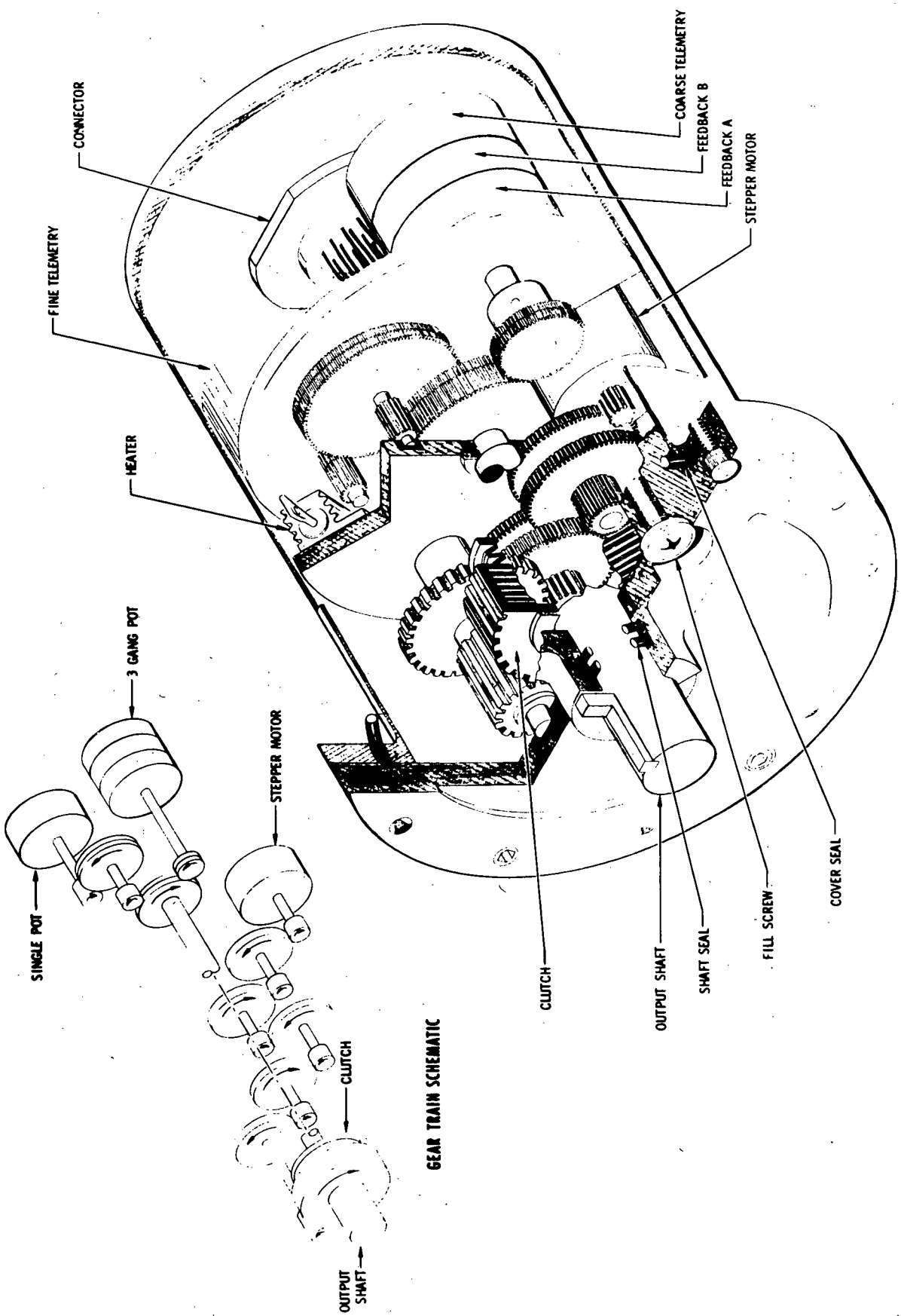

Fig. 33. VO75 antenna actuator

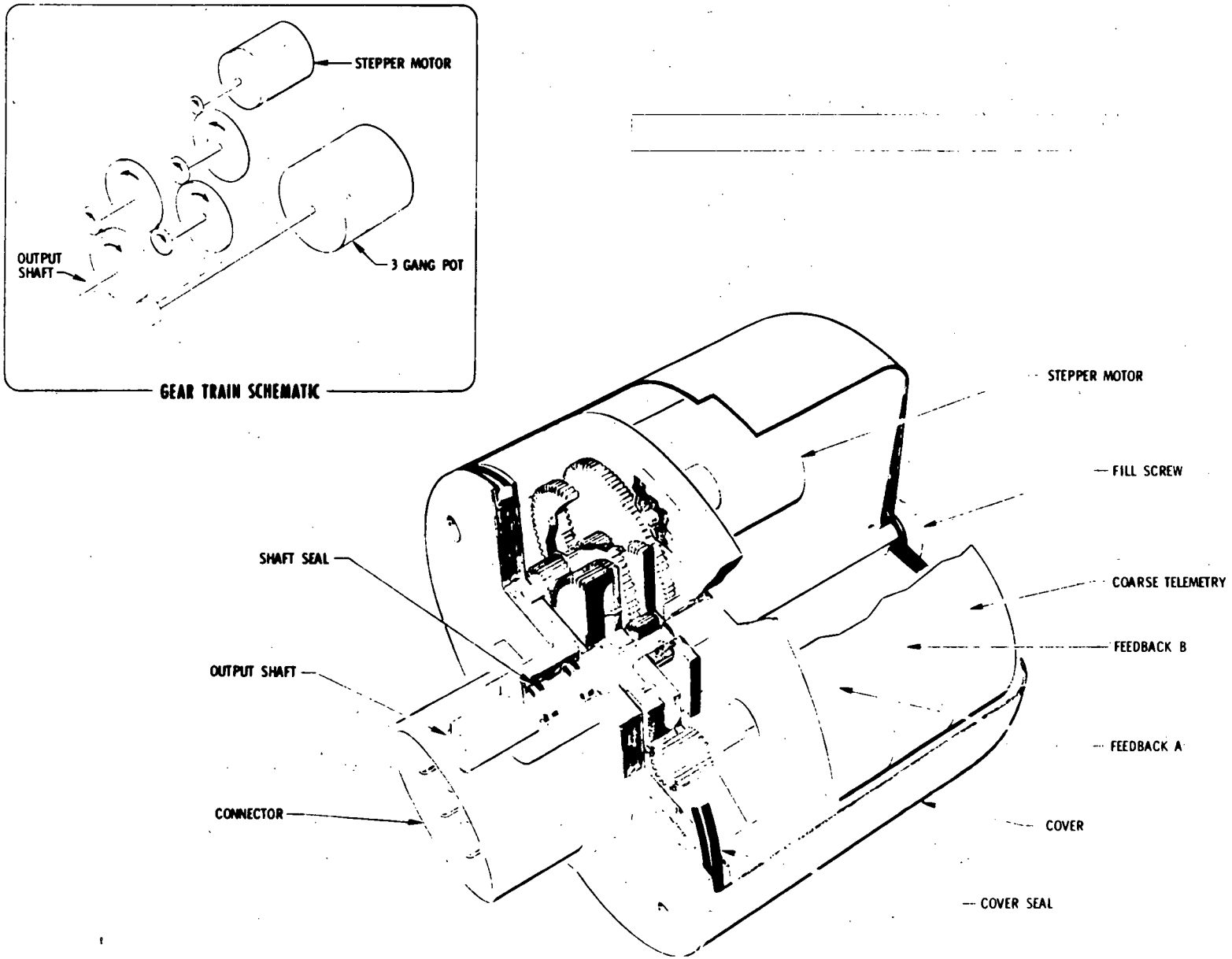

Fig. 34. VO75 solar energy controller actuator

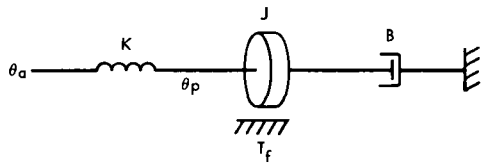

Fig. 35. Simplified platform model

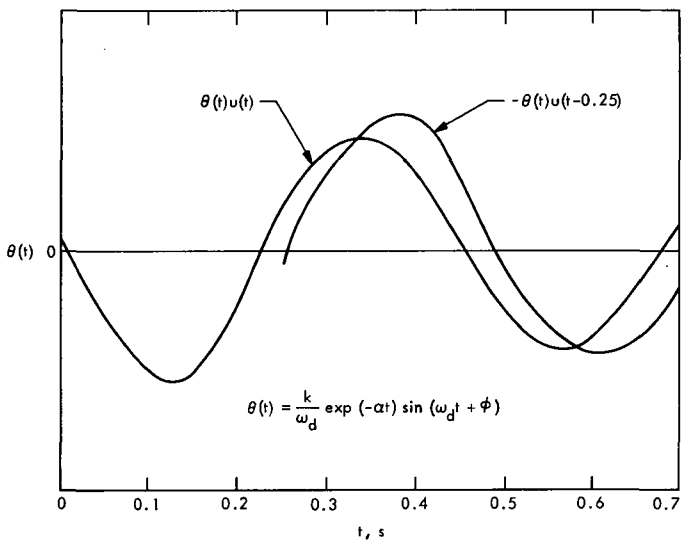

Fig. 36. Near-in-phase transient response, 0.25-deg slew

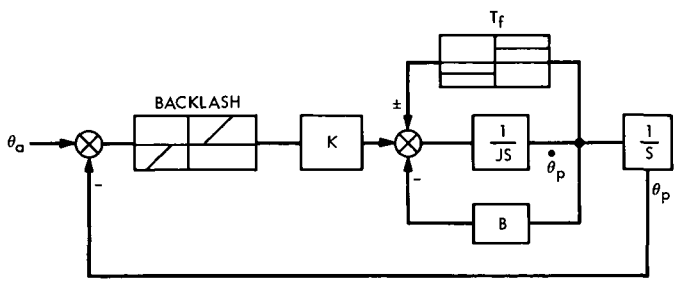

Fig. 37. Block diagram of simplified dynamics model

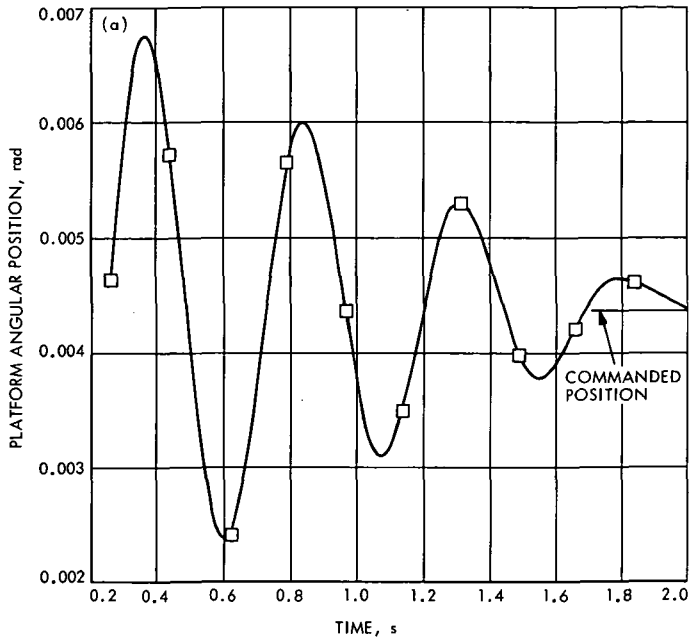

Fig. 38. Platform settling characteristics

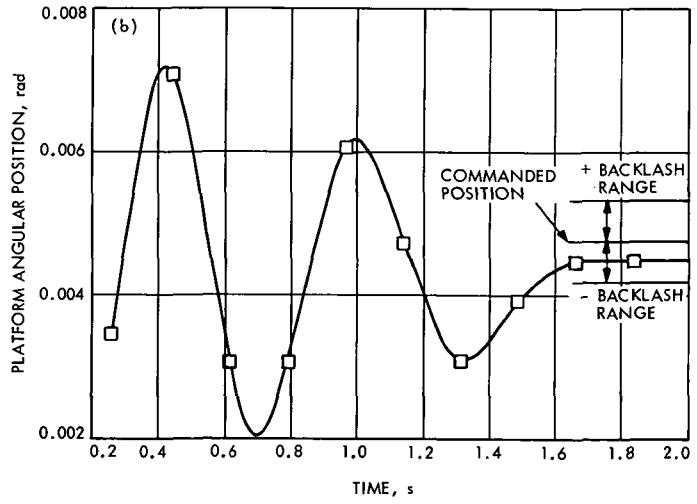

Fig. 38 (contd)

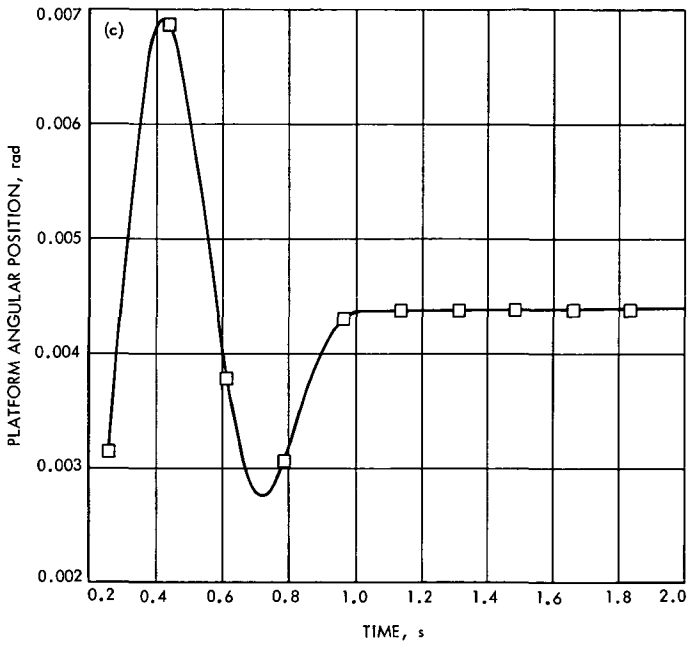

Fig. 38 (contd)

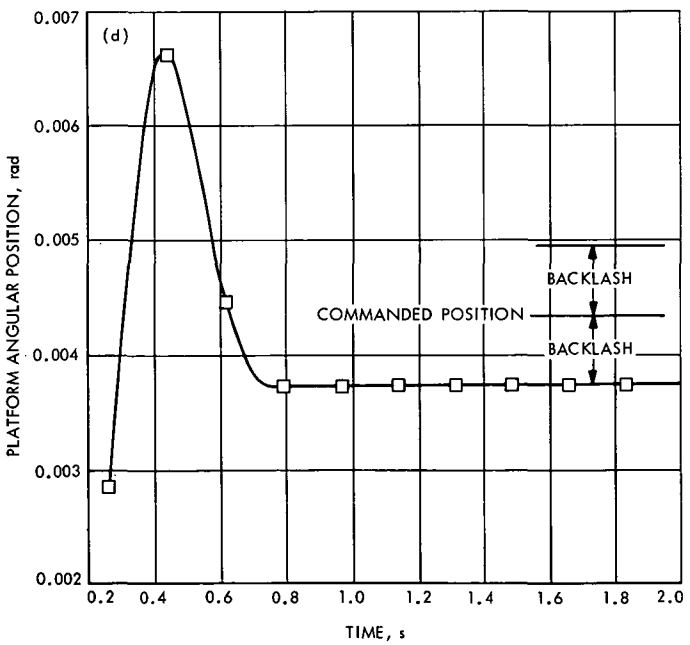

Fig. 38 (contd)

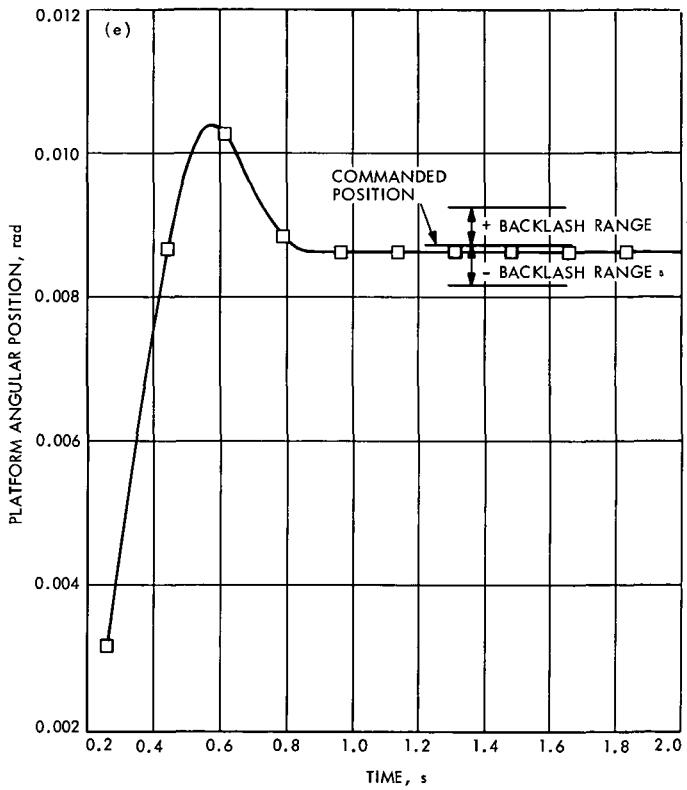
(e)
0.012
0.010
0.008
0.006
0.004
0.002
PLATFORM ANGULAR POSITION, rad
COMMANDED POSITION
+ BACKLASH RANGE
- BACKLASH RANGE
0.2
0.4
0.6
0.8
1.0
1.2
1.4
1.6
1.8
2.0
TIME, s

Fig. 38 (contd)

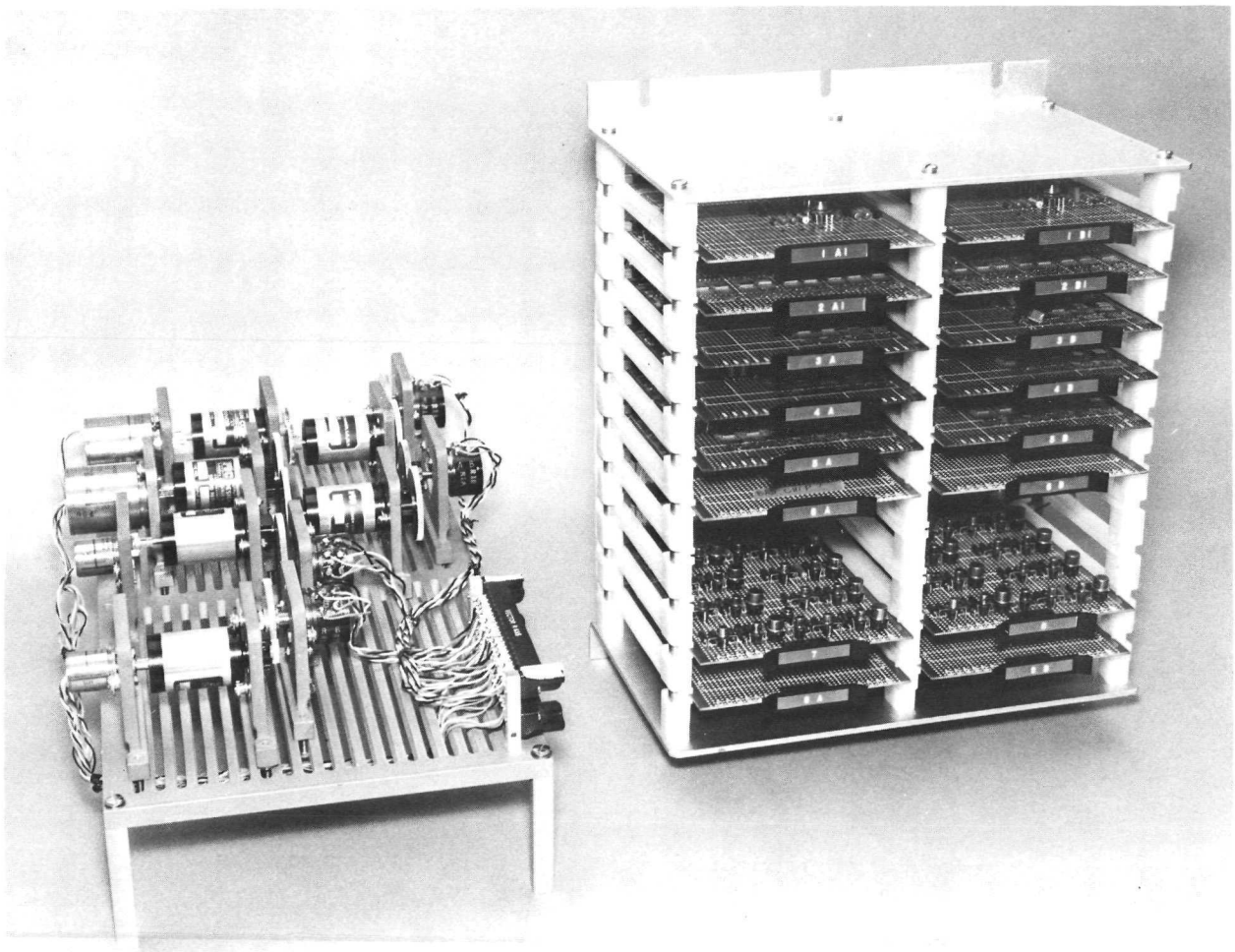

Fig. 39. ARTC breadboard showing two control electronics channels and four actuators

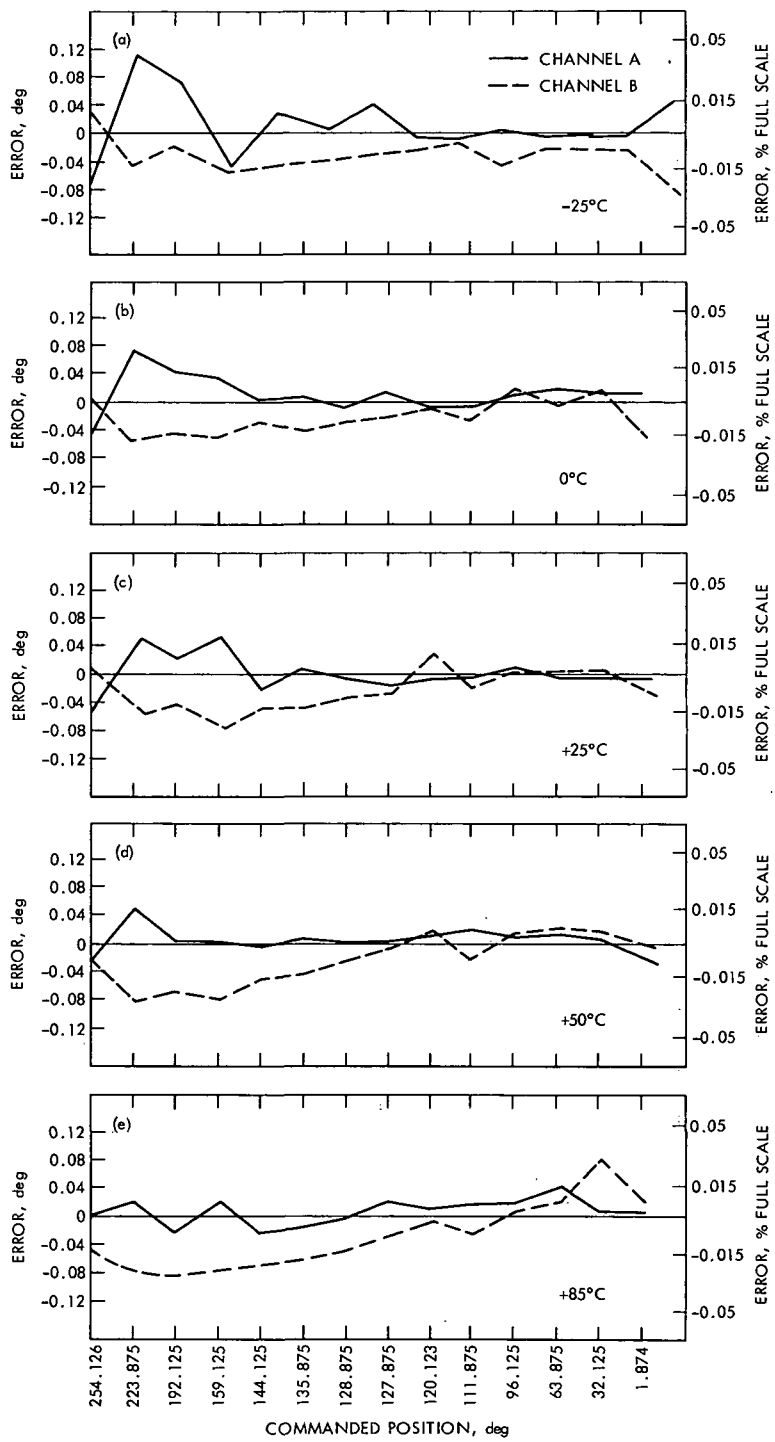

Fig. 40. Position error vs commanded position

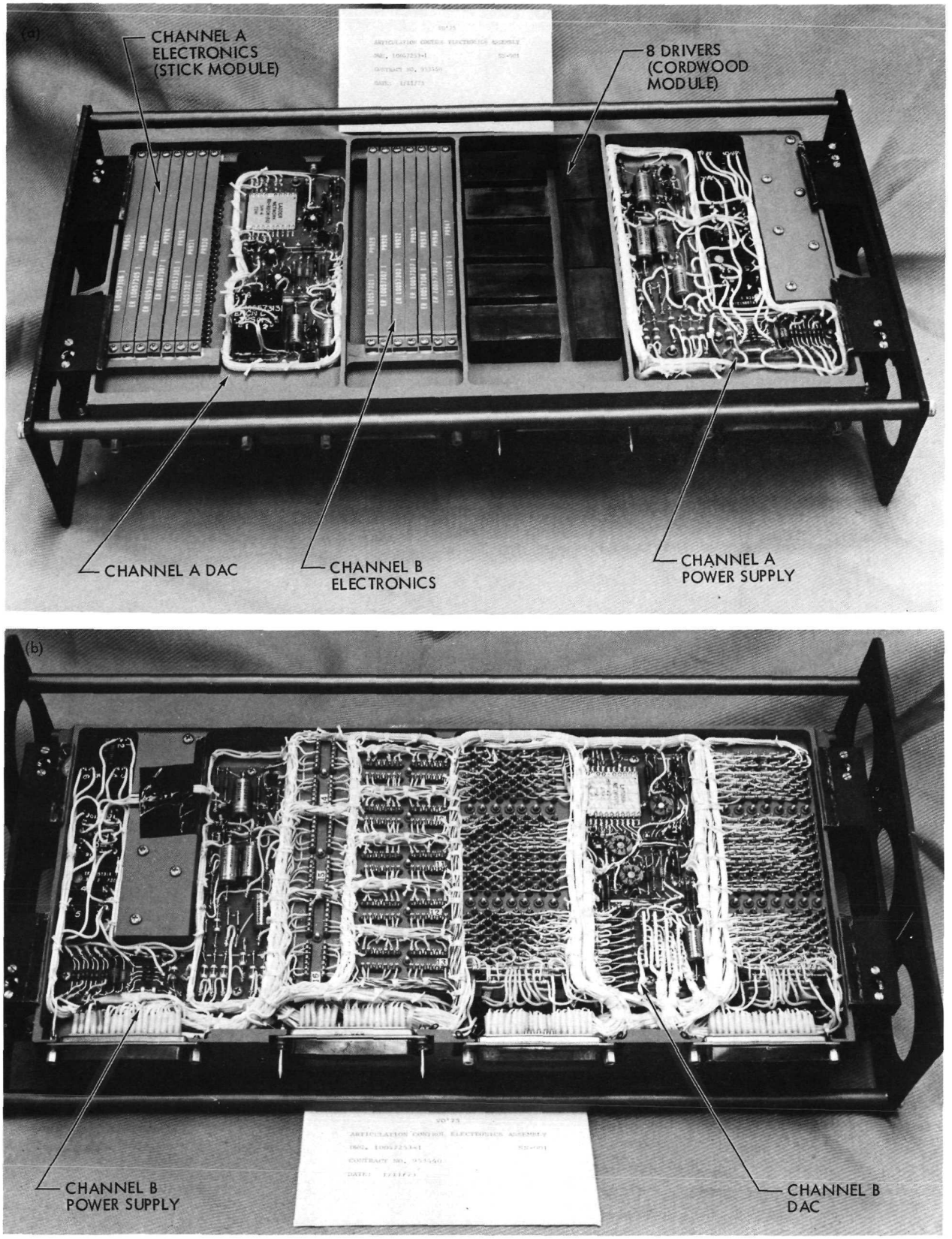

Fig. 41. ARTC electronics production proof model showing (a) the model side, and (b) the harness side.

TECHNICAL REPORT STANDARD TITLE PAGE

1. Report No. 33-599	2. Government Accession No.	3. Recipient's Catalog No.
4. Title and Subtitle VIKING ORBITER 1975 ARTICULATION CONTROL SUBSYSTEM DESIGN AND ANALYSIS		5. Report Date July 15, 1973 6. Performing Organization Code
7. Author(s) H. H. Horiuchi, L. J. Vallas		8. Performing Organization Report No.
9. Performing Organization Name and Address JET PROPULSION LABORATORY California Institute of Technology 4800 Oak Grove Drive Pasadena, California 91103		10. Work Unit No. 11. Contract or Grant No. NAS 7-100 13. Type of Report and Period Covered Technical Memorandum
12. Sponsoring Agency Name and Address NATIONAL AERONAUTICS AND SPACE ADMINISTRATION Washington, D.C. 20546		14. Sponsoring Agency Code

15. Supplementary Notes

16. Abstract

The Articulation Control Subsystem, developed for the Viking Orbiter 1975 spacecraft, is a digital, multiplexed, closed-loop servo system used to control the pointing and positioning of the science scan platform and the high-gain communication antenna, and to position the solar-energy controller louver blades for the thermal control of the propellant tanks. The development, design, and analysis of the Subsystem is preliminary.

The Subsystem consists of a block-redundant control electronics multiplexed among eight control actuators. Each electronics block is capable of operating either individually or simultaneously with the second block. This provides the Subsystem the capability of simultaneous two-actuator control or a single-actuator control with the second block in a stand-by redundant mode.

The result of the preliminary design and analysis indicates that the Subsystem will perform satisfactorily in the Viking Orbiter 1975 mission. Some of the parameter values used, particularly those in the Subsystem dynamics and the error estimates, are preliminary and the results will be updated as more accurate parameter values become available.

17. Key Words (Selected by Author(s))	18. Distribution Statement
Control and Guidance Electronic Components and Circuits Viking Orbiter 1975 Project	Unclassified -- Unlimited

19. Security Classif. (of this report)	20. Security Classif. (of this page)	21. No. of Pages	22. Price
Unclassified	Unclassified	74	

HOW TO FILL OUT THE TECHNICAL REPORT STANDARD TITLE PAGE

Make items 1, 4, 5, 9, 12, and 13 agree with the corresponding information on the report cover. Use all capital letters for title (item 4). Leave items 2, 6, and 14 blank. Complete the remaining items as follows:

3. Recipient's Catalog No. Reserved for use by report recipients.

7. Author(s). Include corresponding information from the report cover. In addition, list the affiliation of an author if it differs from that of the performing organization.

8. Performing Organization Report No. Insert if performing organization wishes to assign this number.

10. Work Unit No. Use the agency-wide code (for example, 923-50-10-06-72), which uniquely identifies the work unit under which the work was authorized. Non-NASA performing organizations will leave this blank.

11. Insert the number of the contract or grant under which the report was prepared.

15. Supplementary Notes. Enter information not included elsewhere but useful, such as: Prepared in cooperation with... Translation of (or by)... Presented at conference of... To be published in...

16. Abstract. Include a brief (not to exceed 200 words) factual summary of the most significant information contained in the report. If possible, the abstract of a classified report should be unclassified. If the report contains a significant bibliography or literature survey, mention it here.

17. Key Words. Insert terms or short phrases selected by the author that identify the principal subjects covered in the report, and that are sufficiently specific and precise to be used for cataloging.

18. Distribution Statement. Enter one of the authorized statements used to denote releasability to the public or a limitation on dissemination for reasons other than security of defense information. Authorized statements are "Unclassified—Unlimited," "U. S. Government and Contractors only," "U. S. Government Agencies only," and "NASA and NASA Contractors only."

19. Security Classification (of report). NOTE: Reports carrying a security classification will require additional markings giving security and downgrading information as specified by the Security Requirements Checklist and the DoD Industrial Security Manual (DoD 5220.22-M).

20. Security Classification (of this page). NOTE: Because this page may be used in preparing announcements, bibliographies, and data banks, it should be unclassified if possible. If a classification is required, indicate separately the classification of the title and the abstract by following these items with either "(U)" for unclassified, or "(C)" or "(S)" as applicable for classified items.

21. No. of Pages. Insert the number of pages.

22. Price. Insert the price set by the Clearinghouse for Federal Scientific and Technical Information or the Government Printing Office, if known.

TECHNICAL REPORT STANDARD TITLE PAGE

1. Report No. 33-599	2. Government Accession No.	3. Recipient's Catalog No.
4. Title and Subtitle		5. Report Date
		6. Performing Organization Code
7. Author(s)		8. Performing Organization Report No.
9. Performing Organization Name and Address JET PROPULSION LABORATORY California Institute of Technology 4800 Oak Grove Drive Pasadena, California 91103		10. Work Unit No. 11. Contract or Grant No. NAS 7-100 13. Type of Report and Period Covered
12. Sponsoring Agency Name and Address NATIONAL AERONAUTICS AND SPACE ADMINISTRATION Washington, D.C. 20546		14. Sponsoring Agency Code
15. Supplementary Notes		

16. Abstract

Overall Viking Project management is the responsibility of the NASA/Langley Research Center; the Jet Propulsion Laboratory is developing the Orbiter System.

17. Key Words (Selected by Author(s))	18. Distribution Statement		
19. Security Classif. (of this report)	20. Security Classif. (of this page)	21. No. of Pages	22. Price

HOW TO FILL OUT THE TECHNICAL REPORT STANDARD TITLE PAGE

Make items 1, 4, 5, 9, 12, and 13 agree with the corresponding information on the report cover. Use all capital letters for title (item 4). Leave items 2, 6, and 14 blank. Complete the remaining items as follows:

3. Recipient's Catalog No. Reserved for use by report recipients.

7. Author(s). Include corresponding information from the report cover. In addition, list the affiliation of an author if it differs from that of the performing organization.

8. Performing Organization Report No. Insert if performing organization wishes to assign this number.

10. Work Unit No. Use the agency-wide code (for example, 923-50-10-06-72), which uniquely identifies the work unit under which the work was authorized. Non-NASA performing organizations will leave this blank.

11. Insert the number of the contract or grant under which the report was prepared.

15. Supplementary Notes. Enter information not included elsewhere but useful, such as: Prepared in cooperation with... Translation of (or by)... Presented at conference of... To be published in...

16. Abstract. Include a brief (not to exceed 200 words) factual summary of the most significant information contained in the report. If possible, the abstract of a classified report should be unclassified. If the report contains a significant bibliography or literature survey, mention it here.

17. Key Words. Insert terms or short phrases selected by the author that identify the principal subjects covered in the report, and that are sufficiently specific and precise to be used for cataloging.

18. Distribution Statement. Enter one of the authorized statements used to denote releasability to the public or a limitation on dissemination for reasons other than security of defense information. Authorized statements are "Unclassified—Unlimited," "U. S. Government and Contractors only," "U. S. Government Agencies only," and "NASA and NASA Contractors only."

19. Security Classification (of report). NOTE: Reports carrying a security classification will require additional markings giving security and downgrading information as specified by the Security Requirements Checklist and the DoD Industrial Security Manual (DoD 5220.22-M).

20. Security Classification (of this page). NOTE: Because this page may be used in preparing announcements, bibliographies, and data banks, it should be unclassified if possible. If a classification is required, indicate separately the classification of the title and the abstract by following these items with either "(U)" for unclassified, or "(C)" or "(S)" as applicable for classified items.

21. No. of Pages. Insert the number of pages.

22. Price. Insert the price set by the Clearinghouse for Federal Scientific and Technical Information or the Government Printing Office, if known.